J Intell Robot Syst (2017) 88:347–377
DOI 10.1007/s10846-017-0528-3

Quadrotor Energy-Based Control Laws: a Unit-Quaternion Approach

M. E. Guerrero-Sánchez · H. Abaunza · P. Castillo · R. Lozano · C. D. García-Beltrán

Received: 15 September 2016 / Accepted: 23 February 2017 / Published online: 28 March 2017

Abstract This article presents the designs, simulations and real-time experimental results of two energy-based control strategies to stabilize an Unmanned Aerial Vehicles (UAV) using a quaternion representation of the attitude. The mathematical model is based on Euler-Lagrange formulation using a logarithmic mapping in the quaternion space. The proposed solutions introduce a new approach: a quaternion-energy-based control, which use an energy-based expression defined as a Lyapunov function. The control laws are described with unit quaternions and their axis-angle representation. The proposed algorithms allow the stabilization of the quadrotor in all its states. The strategies ensure the stability of the closed loop system. Simulation results and experimental validations are developed to verify the effectiveness of the proposed controllers.

Keywords Energy-based control · Quaternion · Quadrotor · Real-time validation · Lyapunov analysis

M. E. Guerrero-Sánchez (✉)
Instituto Tecnológico Superior de Coatzacoalcos,
Carretera Ant. Mina-Coatza Km. 16.5, Col. Las Gaviotas,
CP 96536, Coatzacoalcos, Ver., México
e-mail: maria-eusebia.guerrero-sanchez@utc.fr

H. Abaunza · P. Castillo · R. Lozano
Sorbonne Universités, UTC CNRS UMR 7253
Heudiasyc, Compiègne, France

H. Abaunza
e-mail: habaunza@utc.fr

P. Castillo
e-mail: castillo@utc.fr

R. Lozano
e-mail: rlozano@utc.fr

C. D. García-Beltrán
Centro Nacional de Investigación y Desarrollo
Tecnológico, Interior Internadao Palmira S/N, Palmira,
62490 Cuernavaca, Mor., Mexico
e-mail: cgarcia@cenidet.edu.mx

1 Introduction

Unmanned Aerial Vehicles have experienced a significant development in the last years. Various mathematical models and many control strategies based on classic or modern control theory have been developed for these vehicles. Often, in the major part of the literature on quadrotors, Euler angles are used for the attitude parametrization, which is a very natural way of describing orientation. However, this representation presents inherent singularities and many non-linearities by the use of trigonometric functions, which cause extensive representations of the control algorithms and complications in the design of control strategies. For these reasons, the use of a quaternions instead of Euler angles to model the rotational dynamics and to develop control laws for quadrotors is becoming very popular amongst some researchers.

Few works have investigated the quadrotor attitude control problem using a hyper complex number of rank 4 known as quaternions. For example, in [1]

an approach that utilizes an attitude parametrization based on quaternions is proposed. The strategy consists of two stages. First an input-output linearization from the altitude position to the thrust is performed, followed by a second input-output linearization from the translational position to the control torques. This separation leads to a so called quasi-static feedback linearization that omits additional controller state. Also, in [2] a hierarchical controller design based on non-linear H_∞ theory and backstepping technique is developed for a non-linear and coupled dynamic attitude system using conventional quaternion based method. The derived controller combines the attractive features of H_∞ optimal controller and the advantages of the backstepping technique leading to a control law which avoids winding phenomena.

Similarly, in [3] various control techniques for a quadrotor using a quaternion representation of the attitude were designed. All attitude controllers use a quaternion error to compute control signals that are computed from an actual quaternion and a desired quaternion obtained from a position controller. Attitude and position control laws are obtained using a PD, LQR and backstepping control technique. In [4] the attitude stabilization problem for a quadrotor is considered. Using a new Lyapunov function, an exponentially stabilizing controller based upon the compensation of the Coriolis and gyroscopic torques and the use of a PD feedback structure is derived, where the proportional action is in terms of the vector-quaternion and the two derivative actions are in terms of the airframe angular velocity and the vector-quaternion velocity.

Moreover, in [5] a quaternion-based sliding mode surface is proposed for a model-free of the full dynamic model of a quadrotor. The control algorithm has three important features: the controller assures exponential stability of the full position/attitude dynamics of the system with smooth control efforts, the closed-loop system is robust in presence of external forces and induced moments generated during the flight maneuvers and the controlled quadrotor offers capabilities for aggressive maneuvers. Simulations showed the capabilities of the closed-loop performance under several conditions. Also, [6] proposes a non-linear Proportional squared (P^2) control algorithm fully implemented in the quaternion space, for solving the attitude problem of a quadrotor, the designed control strategy performs very well with a small overshoot and a good reference tracking. However only numerical simulations were presented to prove the efficiency of the suggested scheme.

Meanwhile, [7] introduces the design and experimental flight tests of a quaternion state feedback control scheme to globally stabilize a quadrotor. First an attitude control strategy was proposed to stabilize the vehicle's heading, then a position control law is designed to stabilize the vehicle in all its states. In [8] a comparison between Euler and quaternion approach has been driven, highlighting the efficiency of the second method from a computational point of view. The advantage in considering the quaternion reference is twofold because it avoids critical positions and, it offers a model with the linearity of the coefficients of the transformation matrix, it is also numerically more efficient and stable compared to traditional rotation formulation. Also, in [9] the maximum rate attitude control problem under the input saturation is presented. Moreover, a Backstepping based Inverse Optimal Attitude Controller (BIOAC) is derived wh ich has the property of a maximum convergence rate within the meaning of a control Lyapunov function under input torque limitation. In the controller, a backstepping technique is used for handling the complexity introduced by the unit quaternion representation of the attitude of a quadrotor with four parameters.

Besides, there exist a small number of publications, where an energy-based control is designed for an UAV.

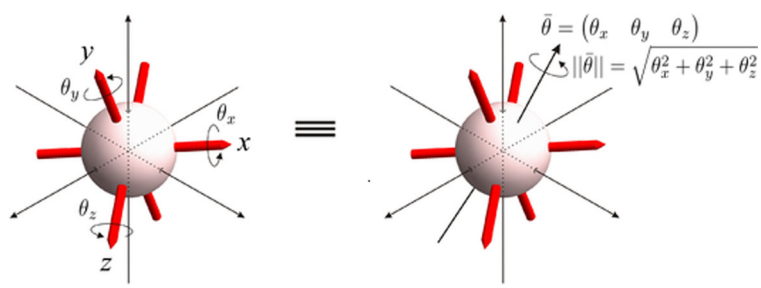

Fig. 1 Axis-angle representation of a rigid body rotation

Fig. 2 Quadrotor scheme

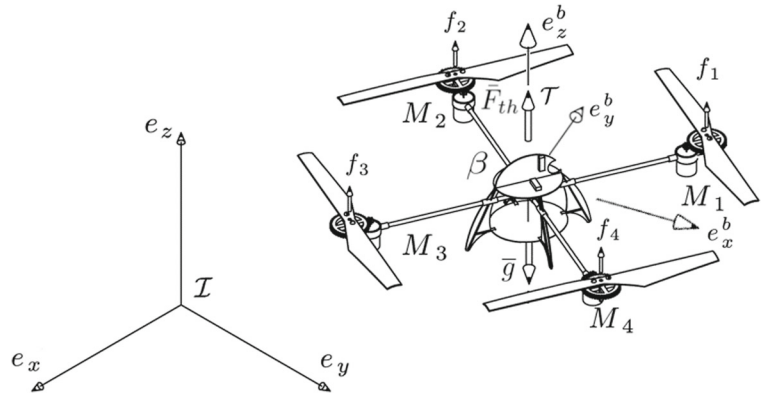

For example in [10] the physical singularities due to under-actuation are solved by using an energy-based control. Energy-based control is used to overcome the lack of controllability of the quadrotor at physical singular configurations, for instance, when commanding the quadrotor to gain altitude while pitched at 90°. Also, in [11] a cascaded non-linear state feedback control law for a quadrotor is presented, which achieves asymptotic tracking of a predefined position and heading reference trajectory. By a suitable shaping of the potential energy and the injection of a sophisticated damping, this approach enables us to design an outer-loop position controller, which satisfies constraints on the maximal and minimal thrust force.

Also, [12] presents a Passivity-Based Control (PBC) to stabilize the quadrotor vehicle. However, the authors reduce the problem to the planar maneuvers case to avoid solving complicated Partial Differential Equations (PDEs). Similarly, in [13], a nonlinear control technique based on passivity to solve the path tracking problem for the quadrotor is presented, but only one control loop was considered in this work. The authors showed that the PBC formulation leads to a set of partial differential equations constraints due to the under-actuation degree of the system.

Moreover, [14] introduces a strategy based on a combination of an energy-based and optimal control approaches to stabilize a quadrotor. The system is linearized for solving the well-known Algebraic Riccati Equation (ARE). Simulations have shown that the performance of the proposed control design is satisfactory also in presence of a wind gust perturbation. In [15] a formal method to design a digital inertial control system for quadrotor aircraft is introduced. In particular, it formalizes how to use approximate passive models in order to justify the initial design of energy-based PD controllers.

Therefore in this paper, we propose two control laws to stabilize a quadrotor using energy-based approaches with unit quaternions. The mathematical model based on Euler-Lagrange formulation is written using a quaternion logarithmic mapping. The dynamical model is such that an under-actuated system as a

Fig. 3 Simulation environment for a quadrotor vehicle

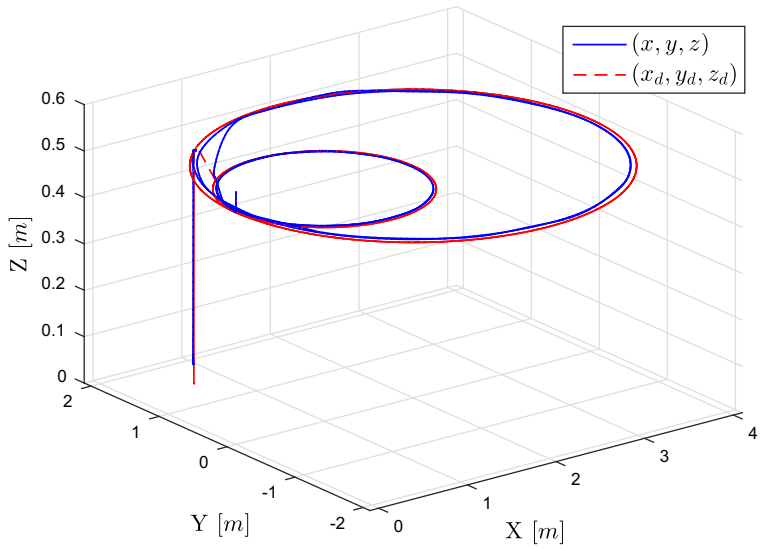

Fig. 4 Quad-rotor's 3-dimensional translation in case 1 simulations, rotated to the North-West-Up convention for a better appreciation

quadrotor can be represented as a fully actuated virtual system. The obtained algorithms are based on an energy function and a desired quaternion trajectory. This allows to control the full dynamics of the vehicle. The presented strategies have no singularity problems and were validated in real-time. Furthermore, external disturbances were added to the experiments, showing an effective compensation while flying.

The paper is structured as follows: a brief background of the main concepts and mathematical expressions used in unit quaternions are presented in Section 2. The quadrotor dynamic model in terms of unit quaternions with the logarithmic mapping is described in Section 3. The energy-based control strategies are developed in Section 4. Numerical simulations to validate the performance of the proposed control strategies are introduced in the Section 5. Real-time experiments are described in Section 6 to demonstrate the performance of our proposals in a real system. Finally, conclusions and future work are discussed in Section 7.

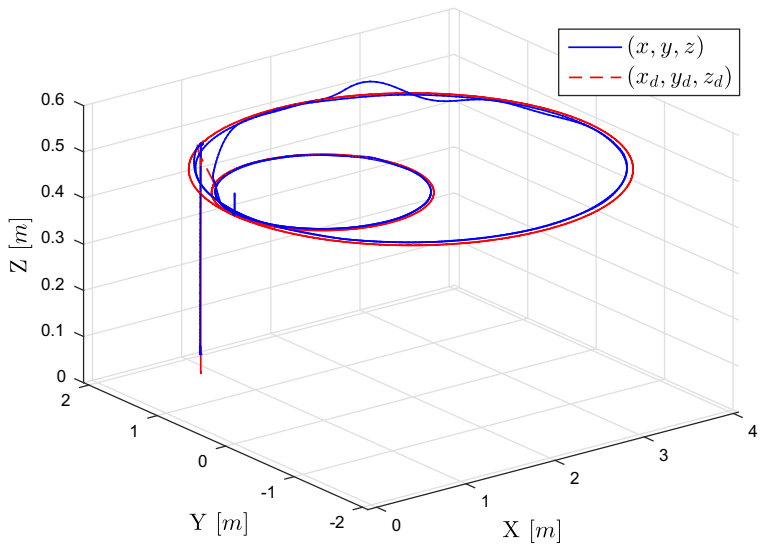

Fig. 5 Quad-rotor's 3-dimensional translation in case 2 simulations, rotated to the North-West-Up convention for a better appreciation

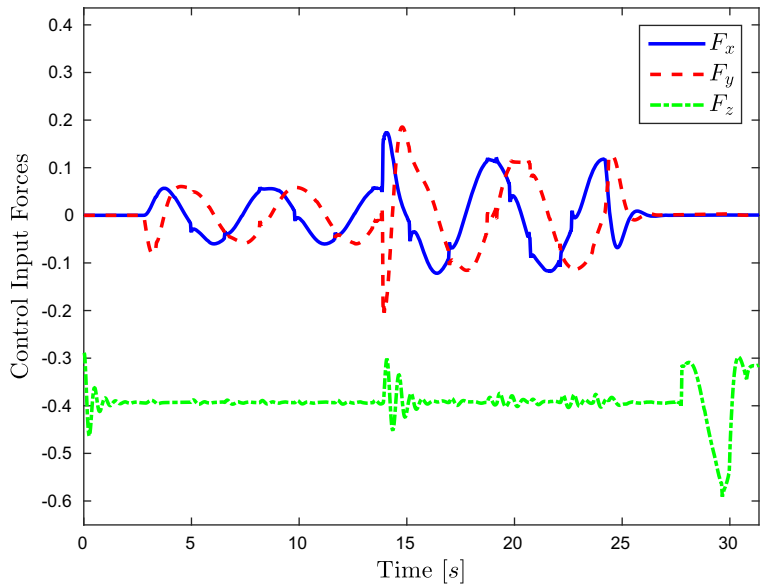

Fig. 6 Input forces for case 1 simulations

2 Quaternion Background

Quaternions are numbers that can be represented as a sum of a scalar component along an imaginary vector. Let $\boldsymbol{q}$ be a quaternion given by [16–19].

$$\boldsymbol{q} = q_0 + \bar{q}, \quad q_0 \in \mathrm{R}, \bar{q} \in \mathrm{R}^3$$

where $\bar{q}$ denotes the complex vectorial part of $\boldsymbol{q}$, and q_0 represents the scalar part of $\boldsymbol{q}$.

Quaternions have several operations such as the product, which is defined by

$$\boldsymbol{q} \otimes \boldsymbol{r} = (q_0 r_0 - \overline{q} \cdot \overline{r}) + (r_0 \overline{q} + q_0 \overline{r} + \overline{q} \times \overline{r}) \quad (1)$$

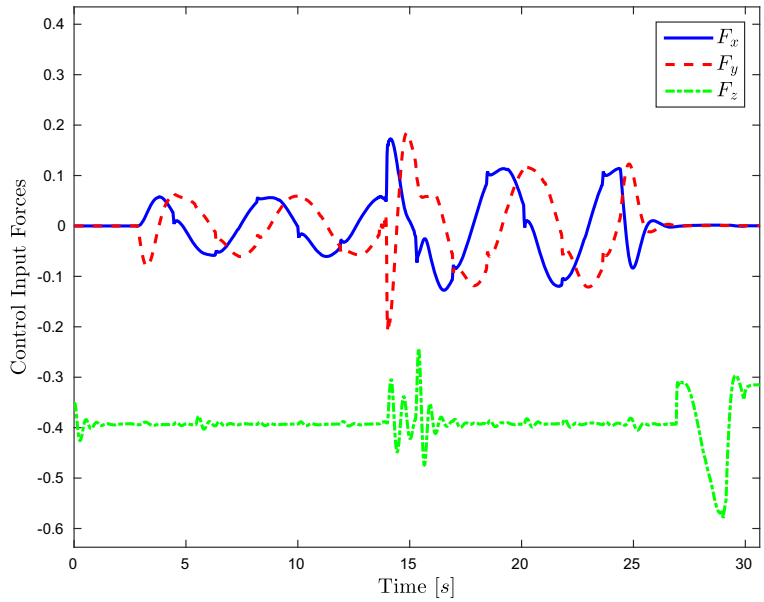

Fig. 7 Input forces for case 2 simulations

Fig. 8 Vehicle's attitude and reference quaternions for case 1 simulations

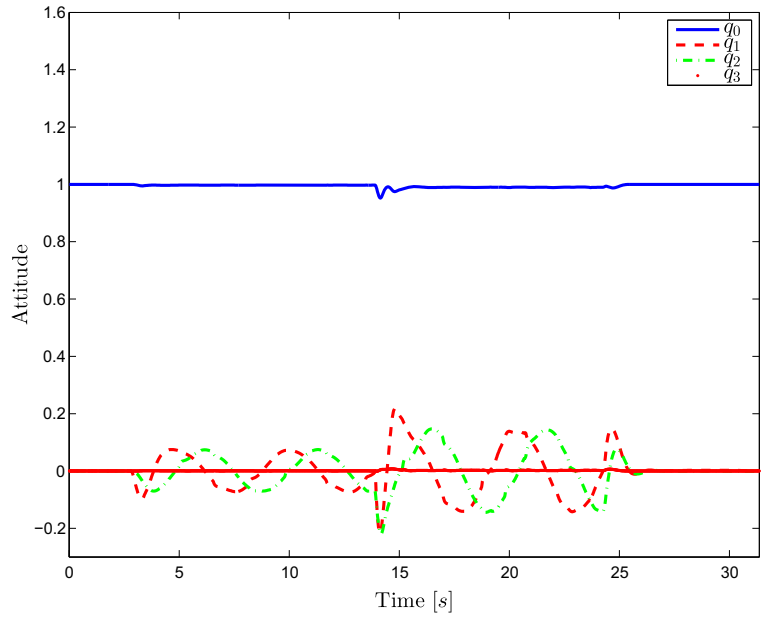

(a) Quad-rotor attitude (q).

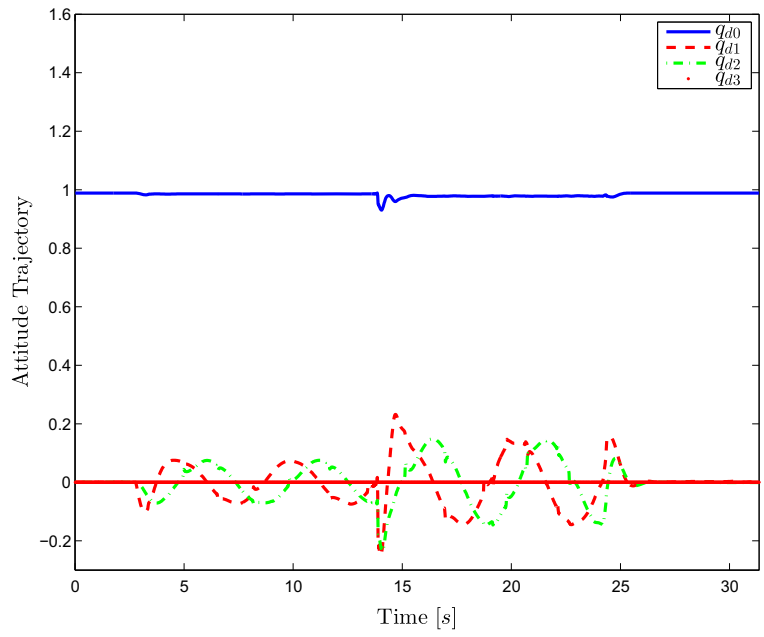

(b) Quad-rotor attitude trajectory (q_d).

where $\boldsymbol{r}$ is also a quaternion. The quaternion conjugate can be expressed as $\boldsymbol{q}^* = q_0 - \overline{q}$, the norm by $||\boldsymbol{q}|| = \sqrt{\boldsymbol{q} \otimes \boldsymbol{q}^*} = \sqrt{q_0^2 + q_1^2 + q_2^2 + q_3^2}$, when $||\boldsymbol{q}|| = 1$, then $\boldsymbol{q}$ is called a unit quaternion. The inverse operator is denoted by $\boldsymbol{q}^{-1} = ||\boldsymbol{q}||^{-1}\boldsymbol{q}^*$. If $\boldsymbol{q}$ is unitary, the inverse and the norm are equivalent.

Fig. 9 Vehicle's attitude and reference quaternions for case 2 simulations

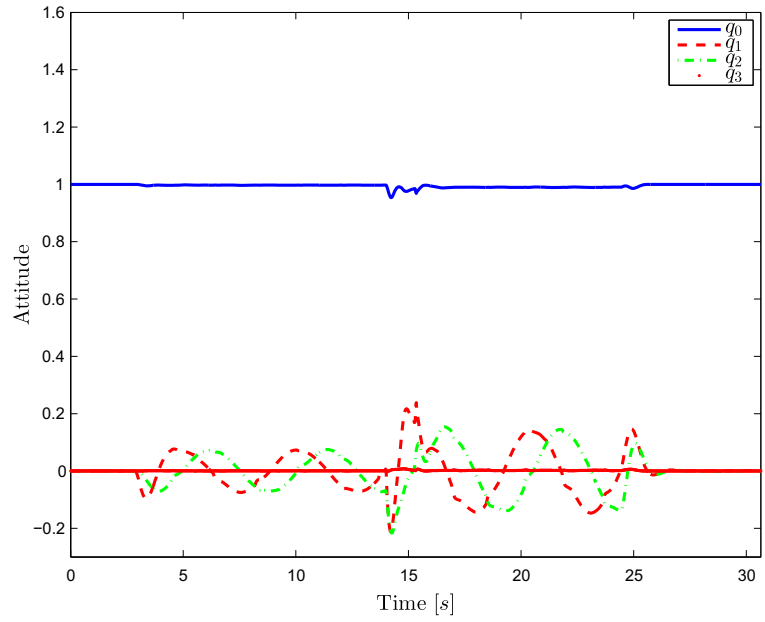

(a) Quad-rotor attitude (q).

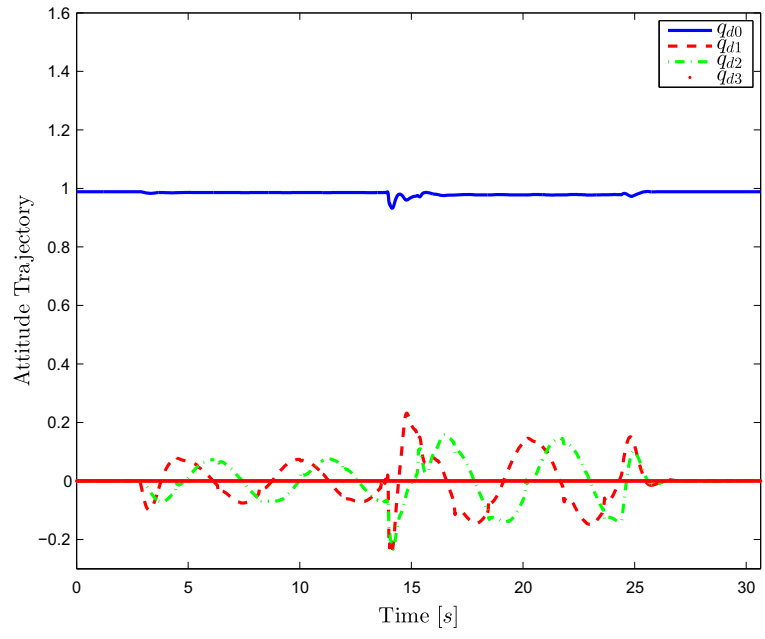

(b) Quad-rotor attitude trajectory (q_d).

A unit quaternion can be used to represent the rotation of a rigid body (see Fig. 1) using the axis-angle representation and the logarithmic mapping

$$\overline{\theta} = 2 \ln \boldsymbol{q}, \quad \dot{\overline{\theta}} = \omega, \tag{2}$$

with

$$\ln \boldsymbol{q} = \begin{cases} \ln ||\boldsymbol{q}|| + \dfrac{\overline{q}}{||\overline{q}||} \arccos \dfrac{q_0}{||\boldsymbol{q}||}, & ||\overline{q}|| \neq 0 \\ \ln ||\boldsymbol{q}||, & ||\overline{q}|| = 0 \end{cases} \tag{3}$$

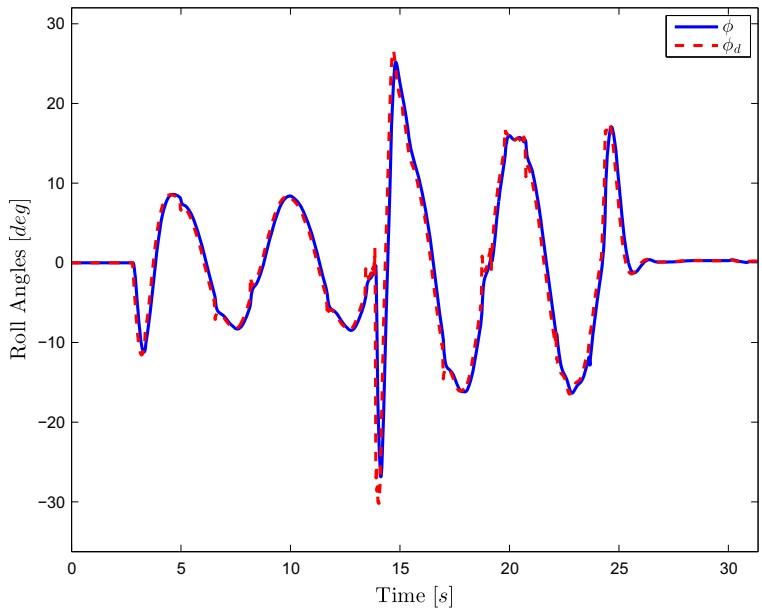

Fig. 10 Attitude and reference for ϕ angles in case 1

Any vector in a 3D space can be rotated from one reference frame (say the inertial frame) to another (for example a body frame) using the expression

$$v' = \boldsymbol{q}^* \otimes v \otimes \boldsymbol{q} \tag{4}$$

where $v \in \mathbb{R}^3$ and $v' \in \mathbb{R}^3$ are in the inertial and body frames respectively.

The derivate of a quaternion which represents the attitude of a rigid body can be expressed in terms of its orientation and its angular velocity as

$$\dot{\boldsymbol{q}} = \frac{1}{2}\boldsymbol{q} \otimes \omega \tag{5}$$

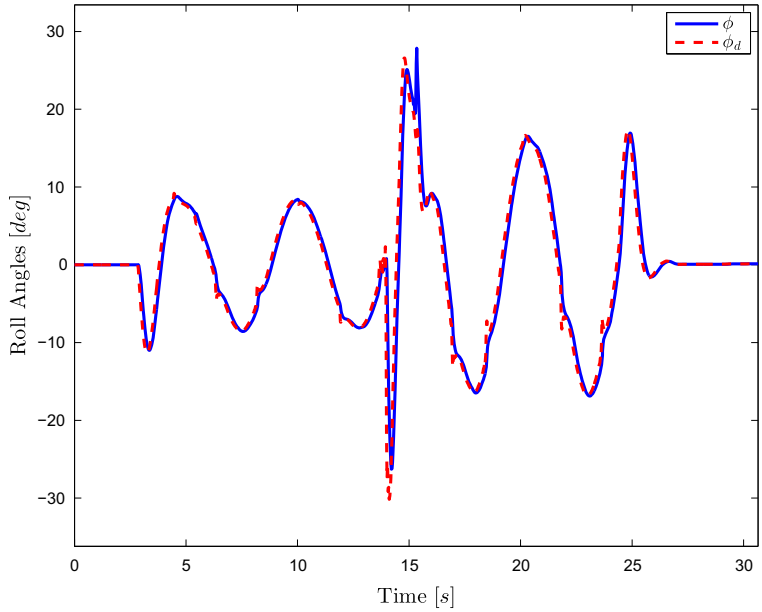

Fig. 11 Attitude and reference for ϕ angles in case 2

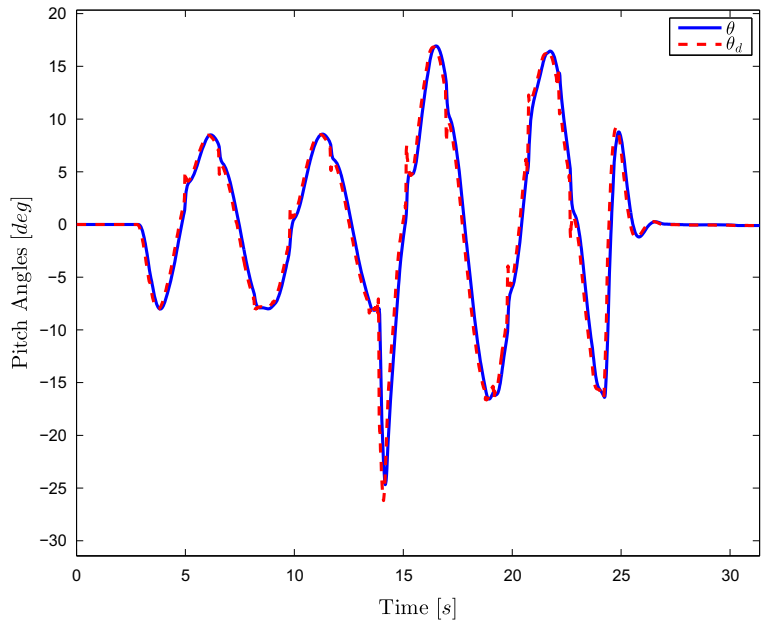

Fig. 12 Attitude and reference for θ angles in case 1

3 Quaternion Mathematical Model

The quadrotor is an under-actuated system with six degrees of freedom and only four control inputs. Figure 2 shows the vehicle scheme.

Let us consider an earth fixed frame $I = \{e_x, e_y, e_z\}$ and body fixed frame $\beta = \{e_x^b, e_y^b, e_z^b\}$, as seen in Fig. 2. $\xi = [\ p\ \bar{\theta}\ ]^T \in \mathbb{R}^6$ denotes all the states variables of the vehicle, where $p = [x\ y\ z]^T$ represents the position vector with respect to the

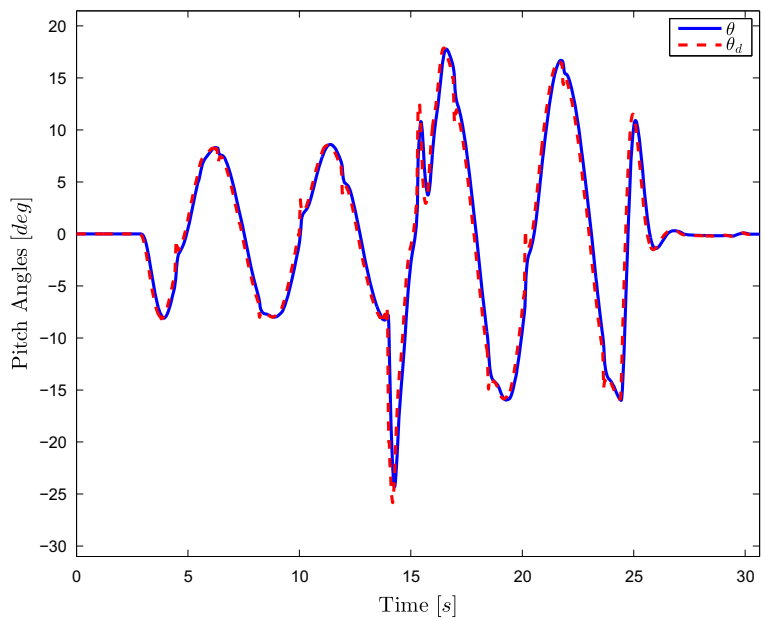

Fig. 13 Attitude and reference for θ angles in case 2

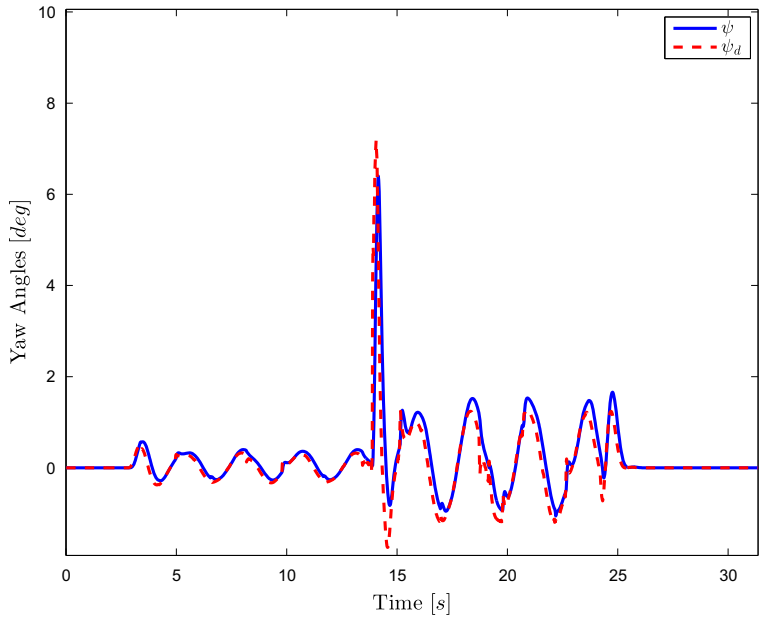

Fig. 14 Attitude and reference for ψ angles in case 1

earth fixed frame, $\bar{\theta} = 2\ln(\boldsymbol{q})$ expresses the rotation quaternion in its axis-angle notation. The vector $\bar{F}_{th} = \begin{bmatrix}0 & 0 & F_{th}\end{bmatrix}^T$ denotes the thrust vector, $\overline{g} = \begin{bmatrix}0 & 0 & -g\end{bmatrix}^T$ defines the gravity vector, the vector $\tau = \begin{bmatrix}\tau_{u_x} & \tau_{u_y} & \tau_{u_z}\end{bmatrix}^T$ expresses the torques applied to the body's center of mass, represented on the quadrotor in the body fixed frame.

3.1 Euler-Lagrange Formulation

The vehicle motion equations can be obtained by the Euler-Lagrange formulation:

$$\frac{d}{dt}\left(\frac{\partial L}{\partial \dot{\xi}}\right) - \frac{\partial L}{\partial \xi} = U, \tag{6}$$

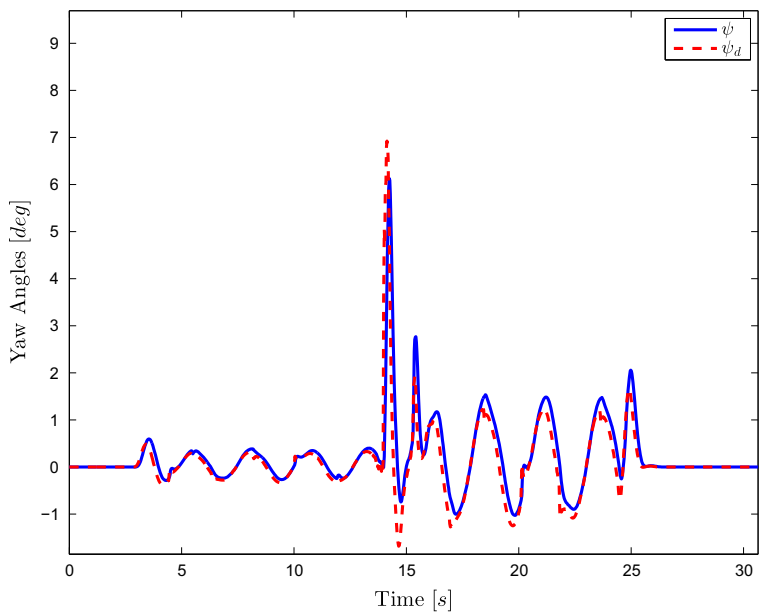

Fig. 15 Attitude and reference for ψ angles in case 2

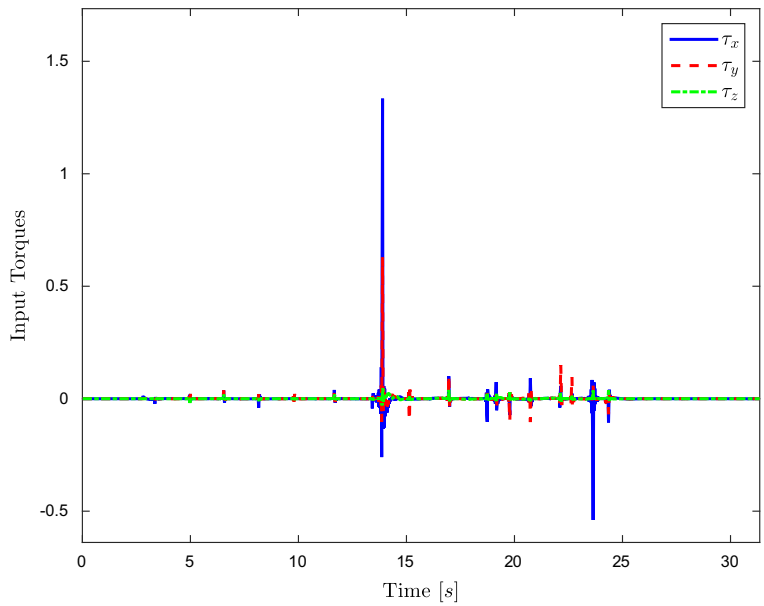

Fig. 16 Input torques for case 1 simulations

where L denotes the Lagrangian of the system and is defined as the difference between the kinetic and potential energy,

$$L(\xi, \dot{\xi}) = K(\dot{\xi}) - V(\xi), \tag{7}$$

$U = [F_u^T \ \tau_u^T]^T$ defines the input vector, which contains F_u that denotes the input force with respect to the earth fixed frame and τ_u that represents the input torques expressed in the body fixed frame.

From Eq. 7, $K(\dot{\xi})$ expresses the total kinetic energy, which is obtained as follows

$$K(\dot{\xi}) = \frac{1}{2} m \dot{p}^T \dot{p} + \frac{1}{2} \dot{\bar{\theta}}^T J \dot{\bar{\theta}} \tag{8}$$

and $V(\xi)$ is the total potential energy of the vehicle

$$V(\xi) = mgz \tag{9}$$

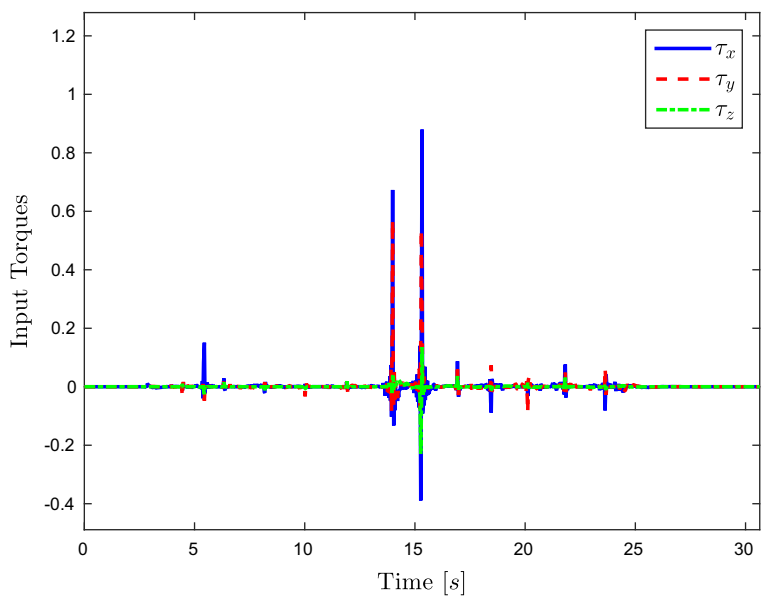

Fig. 17 Input torques for case 2 simulations

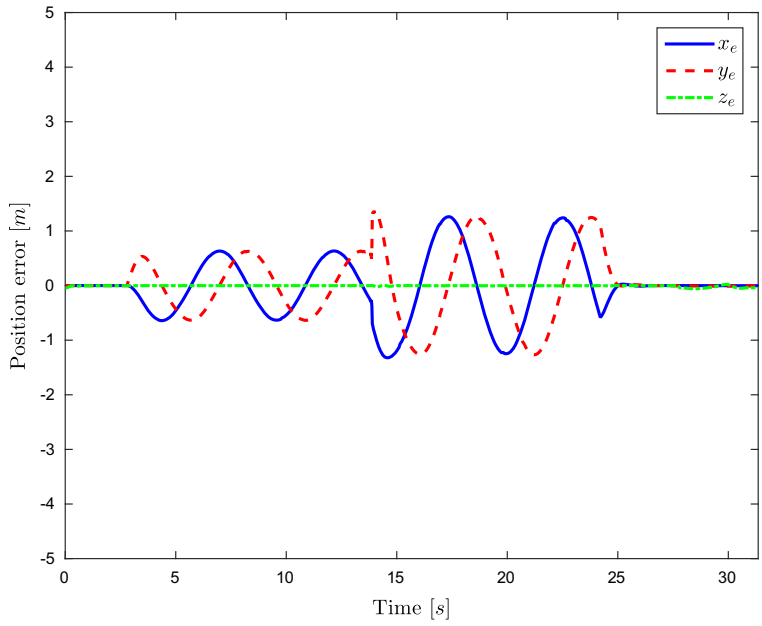

Fig. 18 Position error for case 1 simulations

where m represents the quadrotor's mass, J denotes the inertia matrix, g is the gravity, and z describes the vertical position of the vehicle.

Introducing Eqs. 8 and 9 into Eq. 7 we can obtain the Lagrangian equation as follows

$$L = \frac{1}{2} m \dot{p}^T \dot{p} + \frac{1}{2} \dot{\bar{\theta}}^T J \dot{\bar{\theta}} - mgz, \tag{10}$$

Then, substituting Eq. 10 into Eq. 6 the motion equations can be expressed as

$$\begin{bmatrix} F_u \\ \tau_u \end{bmatrix} = \begin{bmatrix} m\ddot{p} - m\bar{g} \\ J\ddot{\bar{\theta}} \end{bmatrix} \tag{11}$$

where $\ddot{\bar{\theta}} = \tau - \omega \times J\,\omega$.

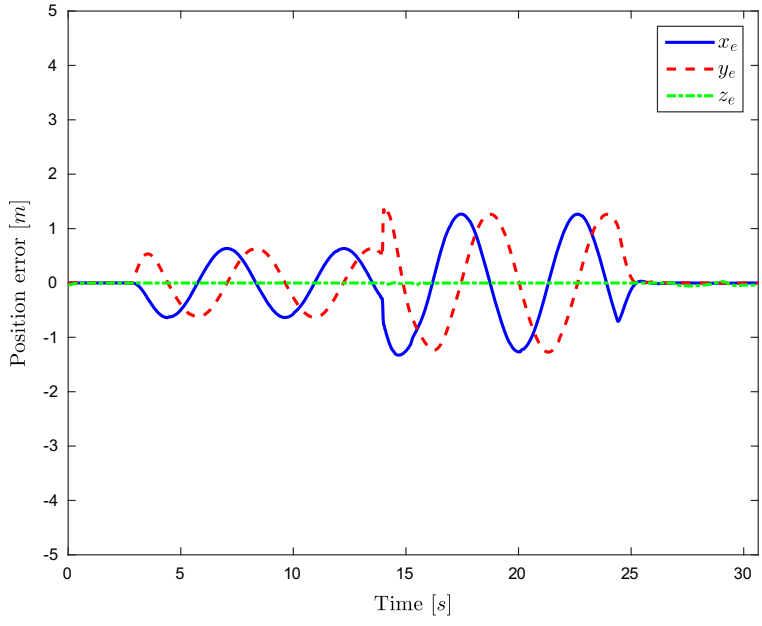

Fig. 19 Position error for case 2 simulations

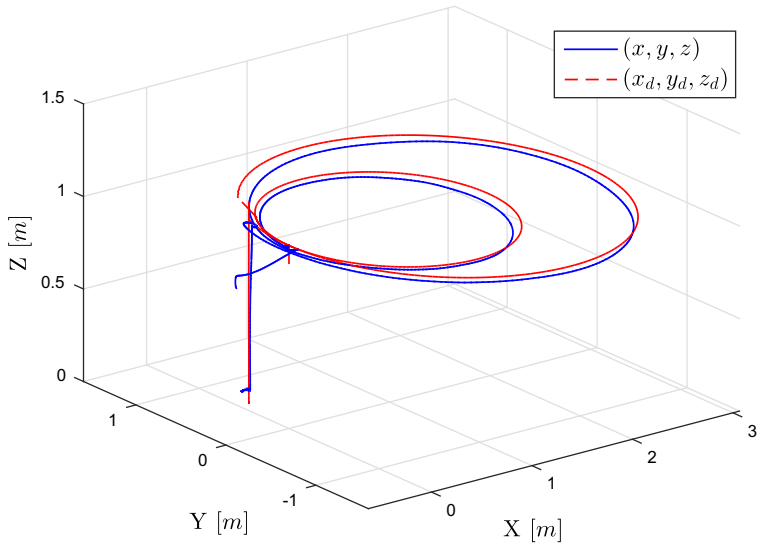

Fig. 20 Quad-rotor's 3-dimensional translation in case 1 experiments

Remember that the quadrotor is an under-actuated system, then the force F_u which is expressed in the earth fixed frame, is the force $\bar{F}_{th}$ rotated, see Eq. 4, therefore

$$F_u = \boldsymbol{q} \otimes \frac{\bar{F}_{th}}{m} \otimes \boldsymbol{q}^* \tag{12}$$

Since the angular acceleration is given by the external torques and the internal rotational dynamics, it can be expressed as

$$\ddot{\bar{\theta}} = \tau - \omega \times J\,\omega \Rightarrow \tau_u = J\,(\tau - \omega \times J\,\omega)\,. \tag{13}$$

Besides, the dynamic model (11) can be expressed in matrix form as

$$M\ddot{\xi} + G = BU, \tag{14}$$

where $M \in \mathbb{R}^{6\times6}$ represents the inertia matrix which is symmetric and positive definite, $G \in \mathbb{R}^{6\times1}$ defines the gravitational vector and finally, $B \in \mathbb{R}^{6\times6}$ is the identity matrix. These matrices are expressed as follows

$$M = \begin{bmatrix} mI_{3\times3} & 0_{3\times3} \\ 0_{3\times3} & I_pI_{3\times3} \end{bmatrix} \tag{15}$$

$$G = \begin{bmatrix} 0 & 0 & mg & 0 & 0 & 0 \end{bmatrix}^T \tag{16}$$

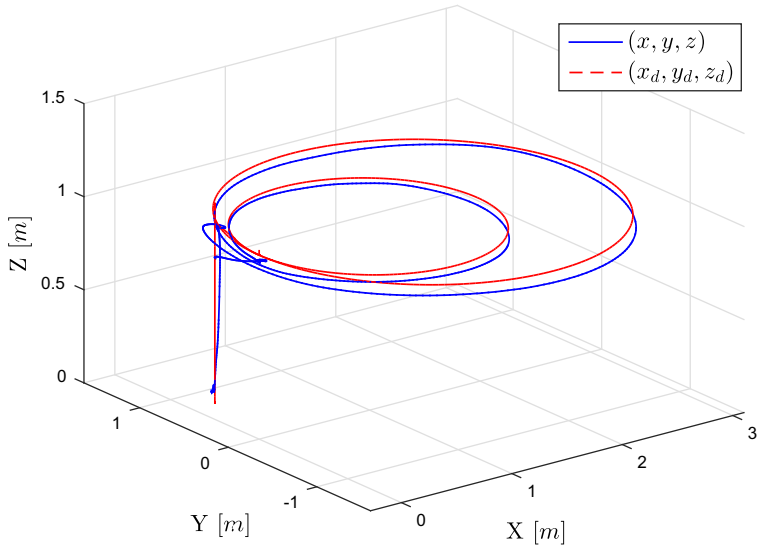

Fig. 21 Quad-rotor's 3-dimensional translation in case 2 experiments

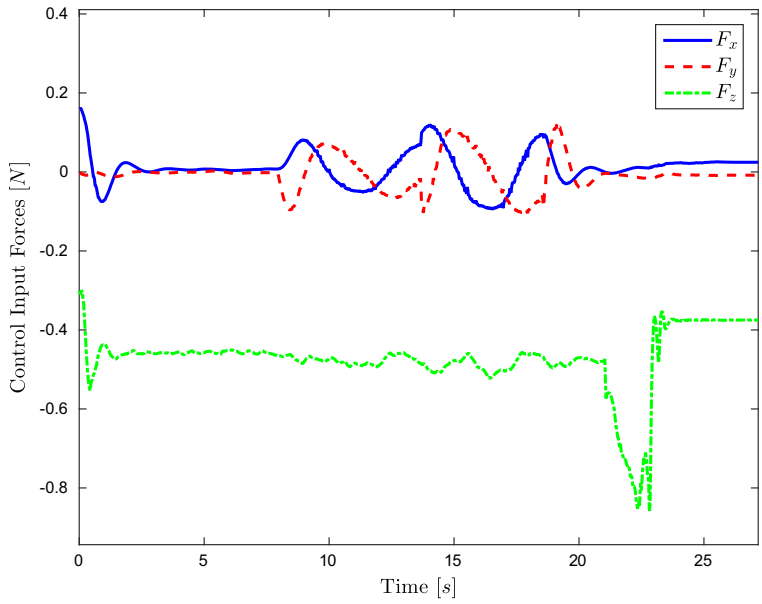

Fig. 22 Quad-rotor's control forces for case 1

where I_p denotes the mass moments of the inertia of the vehicle.

Note from Eq. 12 that the force in the inertial frame depends on the orientation given by $\boldsymbol{q}$, which varies according to the input torque τ as seen in Eq. 13.

4 Quaternion-Energy-Based Control Laws

In this section, the synthesis of the controllers is described.

First, the total energy of the vehicle is obtained and can be described by

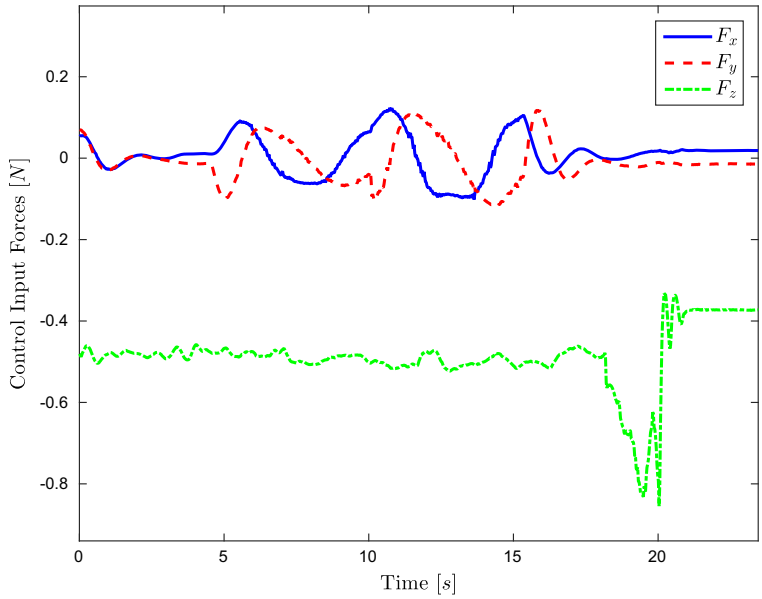

Fig. 23 Quad-rotor's control forces for case 2

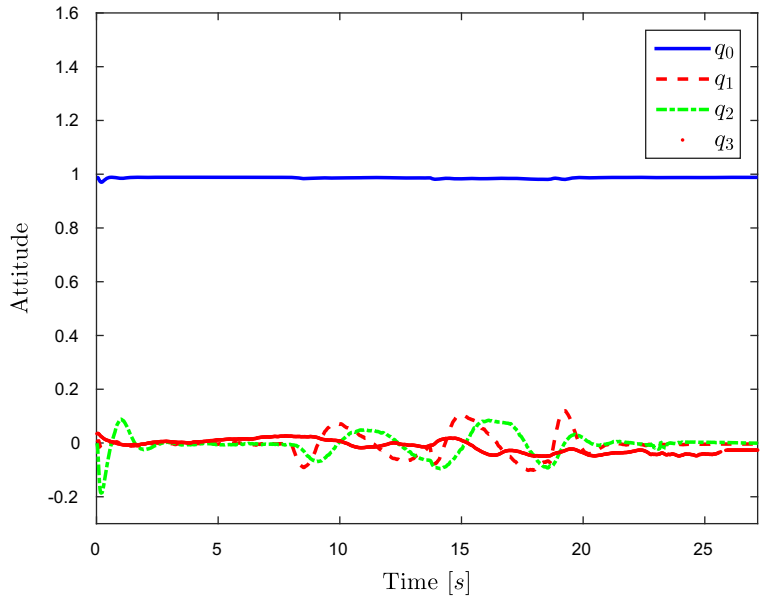

(a) Quad-rotor attitude (q).

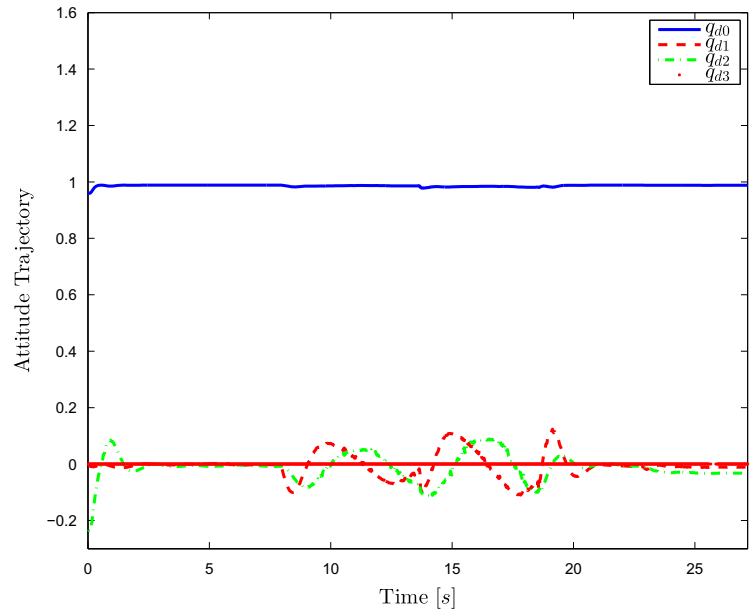

(b) Quad-rotor attitude trajectory (q_d).

Fig. 24 Vehicle's attitude and reference quaternions for case 1 simulations, note the similarity between both graphs

$$H(\xi,\dot{\xi}) = \frac{1}{2}\dot{\xi}^T M\dot{\xi} + V(\xi) \tag{17}$$

In term of the error function, the total energy is described as

$$\bar{H}(\bar{\xi},\dot{\bar{\xi}}) = \frac{1}{2}\dot{\bar{\xi}}^T M\dot{\bar{\xi}} + V(\bar{\xi}) \tag{18}$$

with $\bar{\xi} = \xi - \xi_d$, $\dot{\bar{\xi}} = \dot{\xi} - \dot{\xi_d}$, where ξ_d represents the desired state vector.

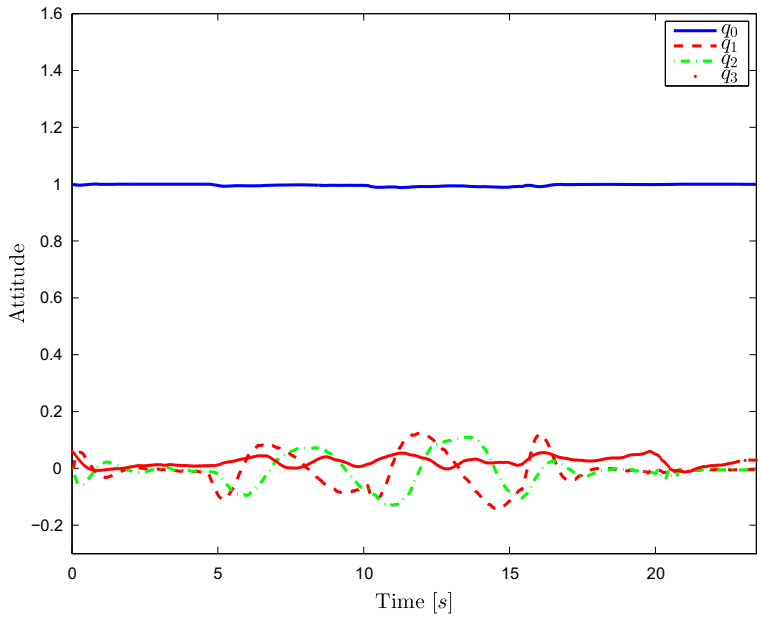

(a) Quad-rotor attitude (q).

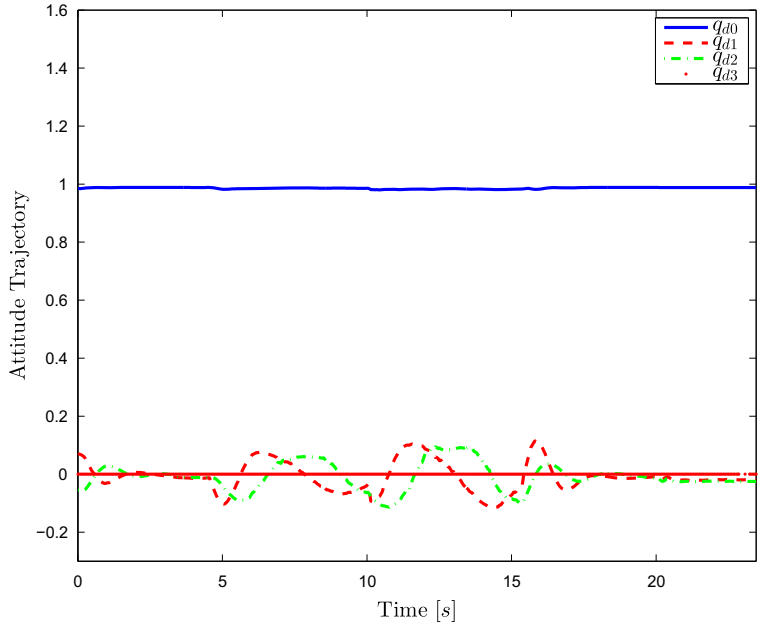

(b) Quad-rotor attitude trajectory (q_d).

Fig. 25 Vehicle's attitude and reference quaternions for case 2 simulations, note the similarity between both graphs

Now, introducing Eq. 9, it yields

$$\bar{H}\bar{\xi},\dot{\bar{\xi}}) = \frac{1}{2}\dot{\bar{\xi}}^T M\dot{\bar{\xi}} + mg\bar{z}$$

Differentiating the above along the trajectories of the system

$$\dot{\bar{H}} = \dot{\bar{\xi}}^T M\ddot{\bar{\xi}} + mg\dot{\bar{z}}$$

From Eq. 16, it follows that

$$\dot{\bar{H}} = \dot{\bar{\xi}}^T M\ddot{\bar{\xi}} + \dot{\bar{\xi}}^T G \tag{19}$$

Substituting Eq. 14 into the above, it follows

$$\dot{\bar{H}} = \dot{\bar{\xi}}^T BU \tag{20}$$

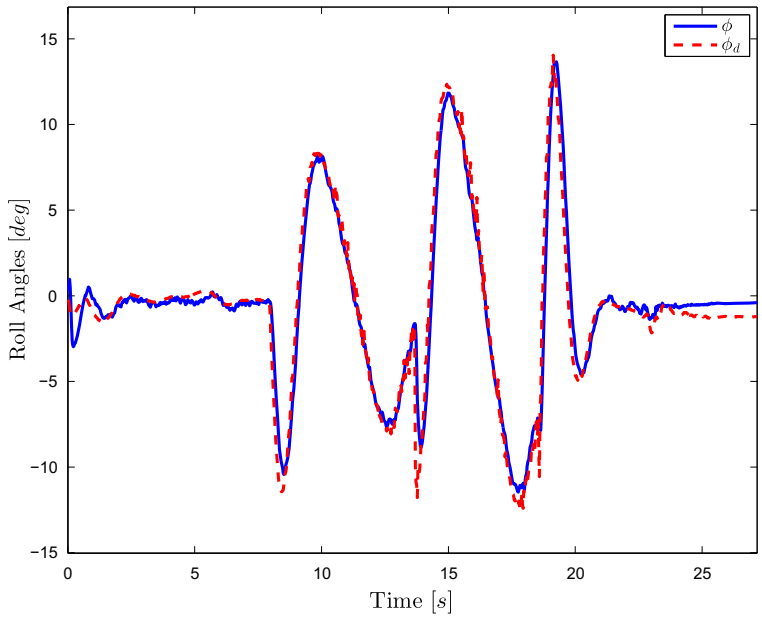

Fig. 26 ϕ angles in case 1 experiments

Two energy-based control schemes are considered in the following subsections.

4.1 Case 1

Now, consider the following positive function as a Lyapunov candidate function

$$V\left(\bar{\xi},\dot{\bar{\xi}}\right) = \frac{1}{2}K_E\bar{H}^2 + \frac{1}{2}\dot{\bar{\xi}}^T K_m\dot{\bar{\xi}} + \frac{1}{2}\bar{\xi}^T K_p\bar{\xi} \quad (21)$$

where $K_p = K_p^T > 0$, $K_m = K_m^T > 0$ and K_E define strictly positive definite constants. Differentiating (21) with respect to time

$$\dot{V}\left(\bar{\xi},\dot{\bar{\xi}}\right) = K_E\bar{H}\dot{\bar{H}} + \dot{\bar{\xi}}^T K_m\ddot{\bar{\xi}} + \dot{\bar{\xi}}^T K_p\bar{\xi}$$

Introducing Eq. 20, we obtain

$$\dot{V}\left(\bar{\xi},\dot{\bar{\xi}}\right) = K_E\bar{H}\dot{\bar{\xi}}^T BU + \dot{\bar{\xi}}^T K_m\ddot{\bar{\xi}} + \dot{\bar{\xi}}^T K_p\bar{\xi}$$

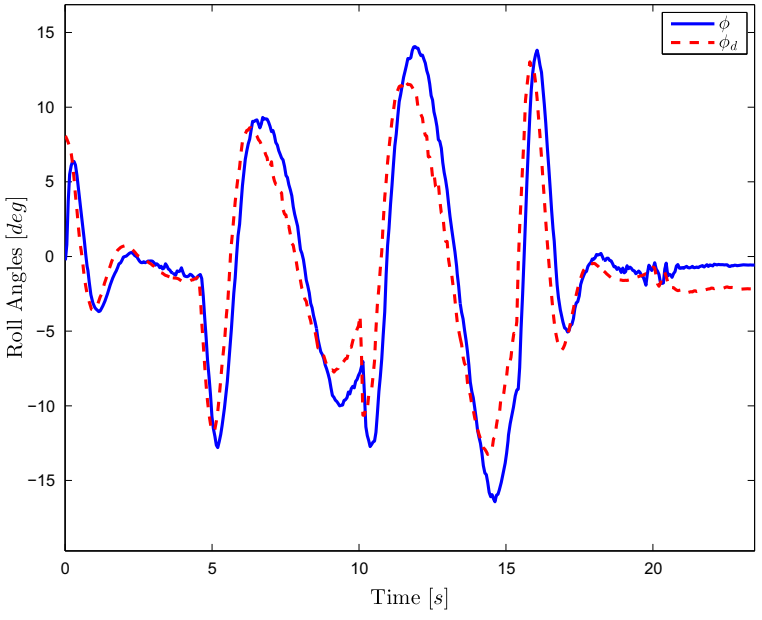

Fig. 27 ϕ angles in case 2 experiments

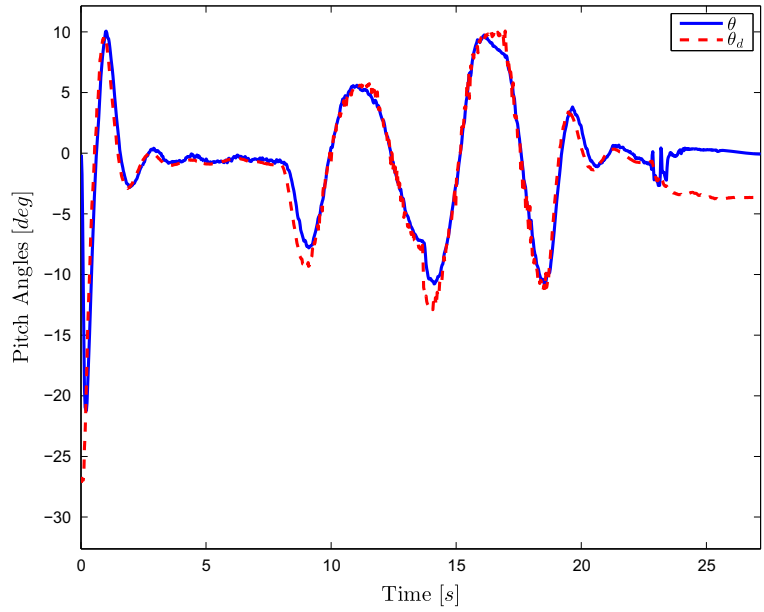

Fig. 28 θ angles in case 1 experiments

Notice from Eq. 14 that $\ddot{\bar{\xi}} = M^{-1}(BU - G)$, then

$$\dot{V} = K_E \bar{H} \dot{\bar{\xi}}^T BU + \dot{\bar{\xi}}^T K_m (M^{-1}(BU - G)) + \dot{\bar{\xi}}^T K_p \bar{\xi}$$

Factoring terms, it follows that

$$\begin{aligned}\dot{V} &= \dot{\bar{\xi}}^T \left(K_E \bar{H} BU + K_m \left(M^{-1} BU - M^{-1} G \right) + K_p \bar{\xi} \right) \\ &= \dot{\bar{\xi}}^T \left(\left[K_E \bar{H} B + K_m M^{-1} B \right] U - K_m M^{-1} G + K_p \bar{\xi} \right)\end{aligned}$$

Therefore, the first control law is defined such that:

$$\left[K_E \bar{H} B + K_m M^{-1} B \right] U - K_m M^{-1} G + K_p \bar{\xi} = -K_v \dot{\bar{\xi}} \tag{22}$$

where $K_v = K_v^T > 0$.

This leads to

$$\dot{V}\left(\bar{\xi}, \dot{\bar{\xi}}\right) = -\dot{\bar{\xi}}^T K_v \dot{\bar{\xi}}$$

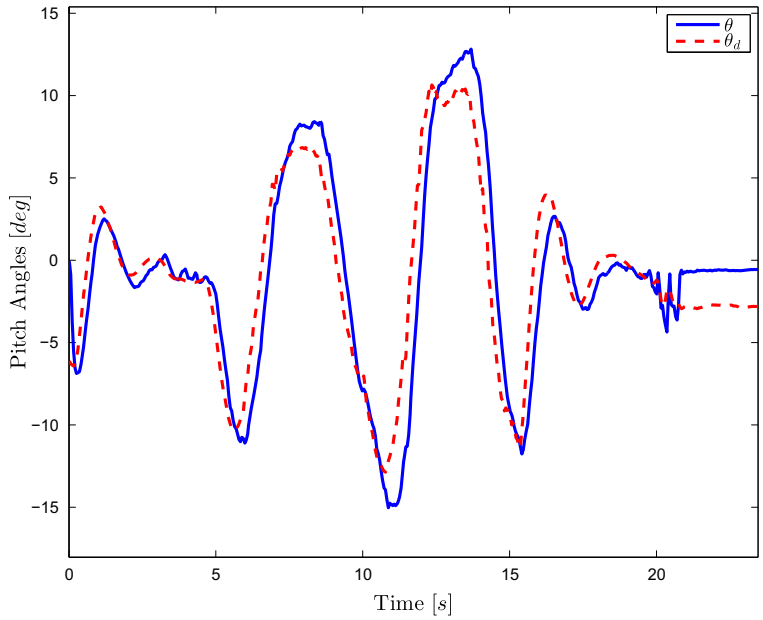

Fig. 29 θ angles in case 2 experiments

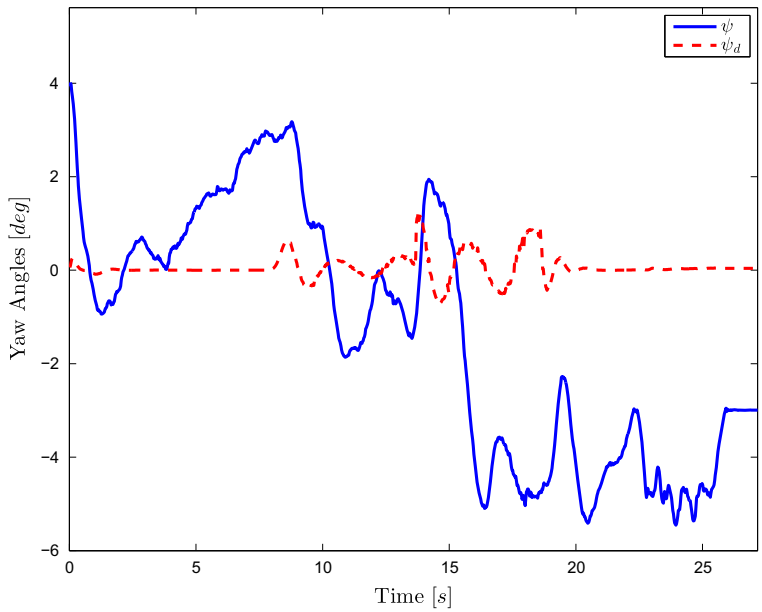

Fig. 30 ψ angles in case 1 experiments

From Eq. 22 we can obtain

$$U = [E]^{-1}\left[-K_p\bar{\xi} - K_v\dot{\bar{\xi}} + K_m M^{-1} G\right]$$

where $E = K_E \bar{H} B + K_m M^{-1} B$.

B is an identity matrix, this ensures that E always has inverse and that U does not have singularities.

The final control law can be rewritten, as follows

$$\begin{bmatrix} F_u \\ \tau_u \end{bmatrix} = [E]^{-1}\begin{bmatrix} -K_{pt}(p - p_d) - K_{vt}(\dot{p} - \dot{p}_d) - K_{mt}\bar{g} \\ -2K_{pr}\ln(\boldsymbol{q}_e) - K_{vr}(\dot{\bar{\theta}} - \dot{\bar{\theta}}_d) \end{bmatrix} \tag{23}$$

where $K_{pt} > 0$, $K_{pr} > 0$, $K_{vt} > 0$, $K_{vr} > 0$ and $K_{mt} > 0$ contain design parameters, p_d denotes

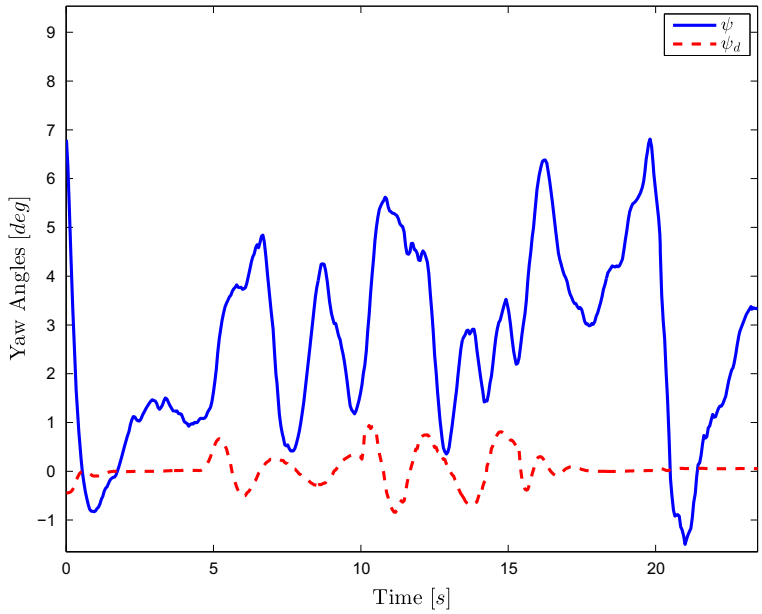

Fig. 31 ψ angles in case 2 experiments

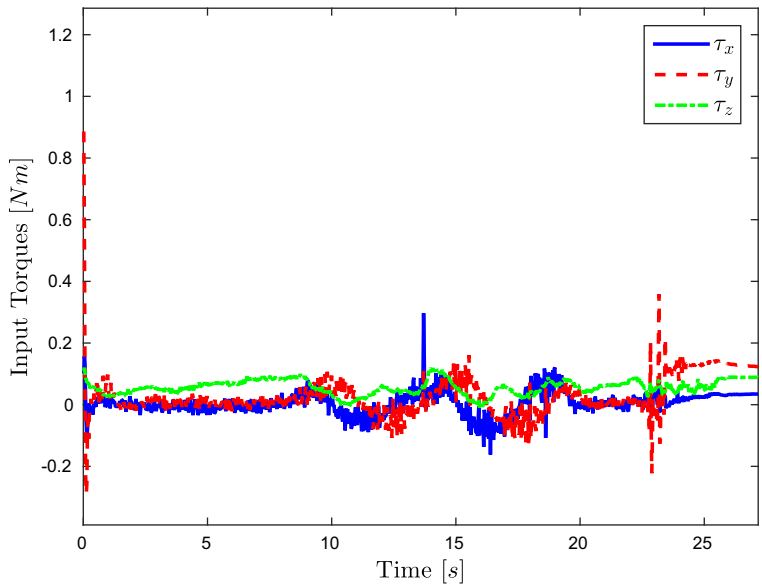

Fig. 32 Quad-rotor's control torques for case 1 tests

the equilibrium configuration, $\bar{\theta}_d = 2 \ln \boldsymbol{q}_d$. Take into account that $\boldsymbol{q}_e = \boldsymbol{q} \otimes \boldsymbol{q}_d^*$ defines the quaternion error between the actual orientation $\boldsymbol{q}$ and the desired reference $\boldsymbol{q}_d^*$. If the control law is such that $\ln(\boldsymbol{q}_e) \rightarrow [0\ 0\ 0]^T$, then $\boldsymbol{q}_e \rightarrow 1 + [0\ 0\ 0]^T$, which implies that the orientation of the vehicle converges to the desired reference $\boldsymbol{q} \rightarrow \boldsymbol{q}_d^*$.

F_u expresses the desired force expressed in the inertial frame which will stabilize the quadrotor in the desired position, and τ_u represents the torque that makes the attitude converge to the desired quaternion reference.

The quaternion trajectory $\boldsymbol{q}_d$ is defined as follows

$$\begin{aligned} \boldsymbol{q}_d &= \frac{(b \cdot F_u + ||F_u||) + b \times F_u}{||(b \cdot F_u + ||F_u||) + b \times F_u||}, \\ F_{th} &= ||F_u|| \end{aligned} \tag{24}$$

where $b = [0\ 0\ 1]^T$ denotes the axis on which the thrust acts in the body fixed frame.

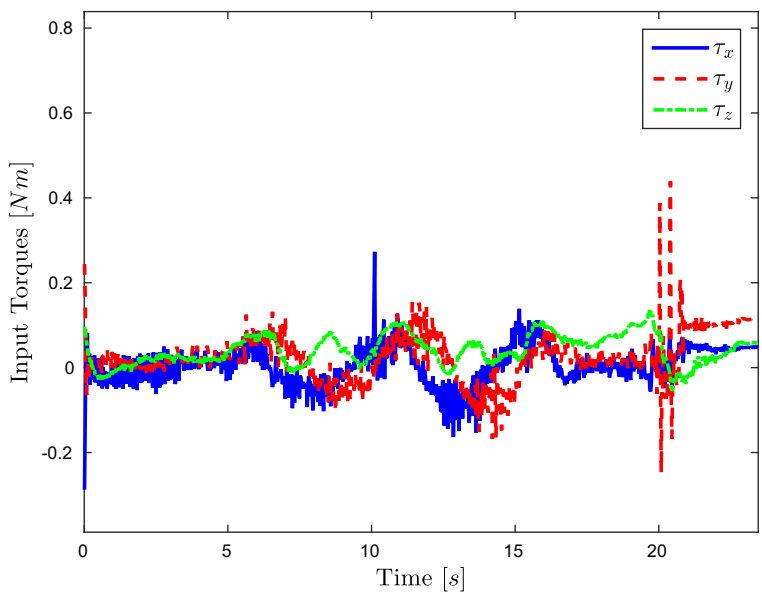

Fig. 33 Quad-rotor's control torques for case 2 tests

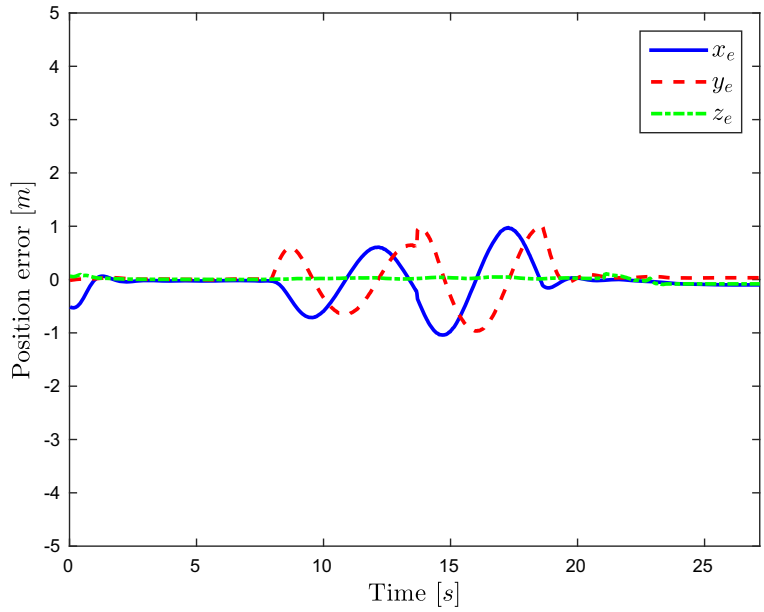

Fig. 34 Quad-rotor's position error in case 1 experiments

From Eq. 24 $\boldsymbol{q}_d$ is used to close the loop such that $\bar{F}_{th}$ is rotated to coincide with F_u, thus the position is stabilized in the desired reference. The above is justified by well known time-scale separation between rotational and translational dynamics. Thus, the control law (23) in quaternion space guarantees the stabilization of all the system states.

4.2 Case 2

In this case an energy-based optimal control law using unit-quaternions is proposed.

Considering the state vector as $x(t) = [\,\bar{\xi}\ \dot{\bar{\xi}}\,]^T = [\,p\ \bar{\theta}\ \dot{p}\ \dot{\bar{\theta}}\,]^T$. Then, system (11) can be rewritten as follows:

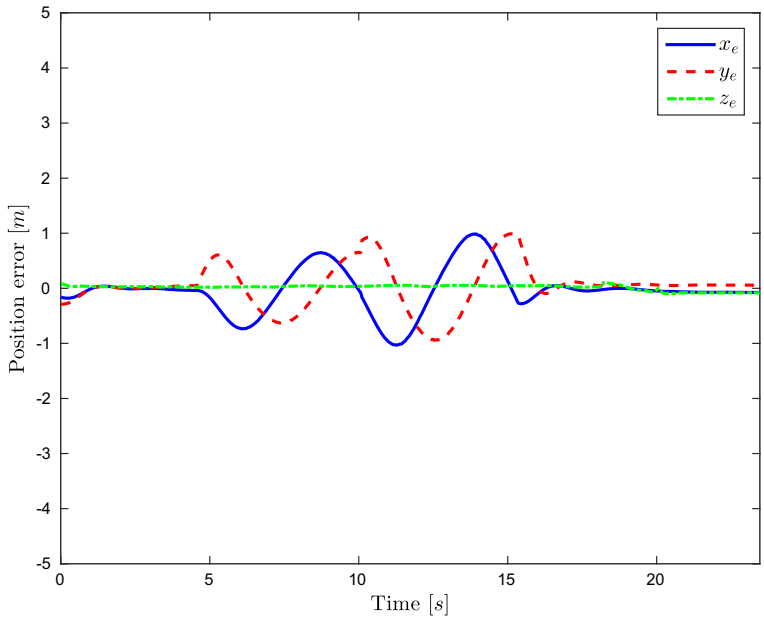

Fig. 35 Quad-rotor's position error in case 2 experiments

Fig. 36 Disturbance caused by one of our team members

$$\begin{bmatrix} \dot{x}_1 \\ \dot{x}_2 \\ \dot{x}_3 \\ \dot{x}_4 \end{bmatrix} = \begin{bmatrix} x_2 \\ x_4 \\ -g \\ 0 \end{bmatrix} + \begin{bmatrix} 0 \\ 0 \\ m^{-1}F_u \\ J^{-1}\tau_u \end{bmatrix} \tag{25}$$

Now, the performance cost function which is to be minimized is defined as follows:

$$J = \frac{1}{2}\int_0^\infty \left(x^T Q x + u^T R u\right) dt \tag{26}$$

where the state and input weighting matrices are assumed such that $Q = Q^T$, $Q > 0$ and $R = R^T$, $R \geqslant 0$.

System (25) can be optimally stabilized solving:

$$\frac{dV_o}{dt} + x^T Q x + u^T R u = 0 \tag{27}$$

Then, consider the following Lyapunov candidate function based on the total energy

$$V_o = \frac{1}{2}K_E \bar{H}^2 + \frac{1}{2}\dot{\bar{\xi}}^T K_m \dot{\bar{\xi}} + \frac{1}{2}\bar{\xi}^T K_p \bar{\xi} + \bar{\xi}^T K_T \dot{\bar{\xi}} \tag{28}$$

where $K_T = {K_T}^T > 0$. Differentiating (28) along the trajectories of the system

$$\begin{aligned} \dot{V}_o\left(\bar{\xi}, \dot{\bar{\xi}}\right) = {} & K_E \bar{H}\dot{\bar{H}} + \dot{\bar{\xi}}^T K_m \ddot{\bar{\xi}} + \dot{\bar{\xi}}^T K_p \bar{\xi} \\ & + \bar{\xi}^T K_T \ddot{\bar{\xi}} + \dot{\bar{\xi}}^T K_T \dot{\bar{\xi}} \end{aligned}$$

Now, introducing (19) in the above, it follows that

$$\begin{aligned} \dot{V}_o = {} & K_E \bar{H}(\dot{\bar{\xi}}^T M \ddot{\bar{\xi}} + \dot{\bar{\xi}}^T G) + \dot{\bar{\xi}}^T K_m \ddot{\bar{\xi}} + \dot{\bar{\xi}}^T K_p \bar{\xi} \\ & + \bar{\xi}^T K_T \ddot{\bar{\xi}} + \dot{\bar{\xi}}^T K_T \dot{\bar{\xi}} \\ = {} & \left(K_E \bar{H}\dot{\bar{\xi}}^T M + \dot{\bar{\xi}}^T K_m + \bar{\xi}^T K_T\right)\ddot{\bar{\xi}} + K_E \bar{H}\dot{\bar{\xi}}^T G \\ & + \dot{\bar{\xi}}^T K_p \bar{\xi} + \dot{\bar{\xi}}^T K_T \dot{\bar{\xi}} \end{aligned} \tag{29}$$

Substituting Eq. 14 into Eq. 29, it yields

$$\begin{aligned} \dot{V}_o = {} & \left(K_E \bar{H}\dot{\bar{\xi}}^T M + \dot{\bar{\xi}}^T K_m + \bar{\xi}^T K_T\right) M^{-1}(U - G) \\ & + K_E \bar{H}\dot{\bar{\xi}}^T G + \dot{\bar{\xi}}^T K_p \bar{\xi} + \dot{\bar{\xi}}^T K_T \dot{\bar{\xi}} \end{aligned} \tag{30}$$

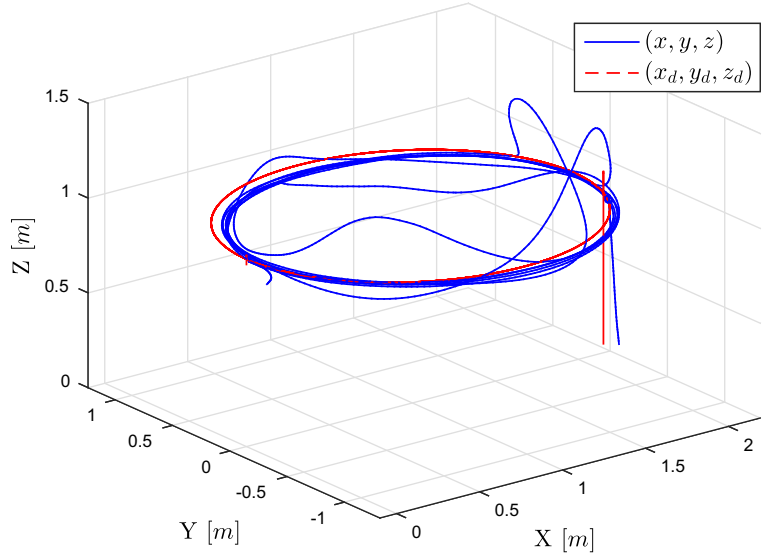

Fig. 37 Quad-rotor's disturbed trajectory in case 1 experiments

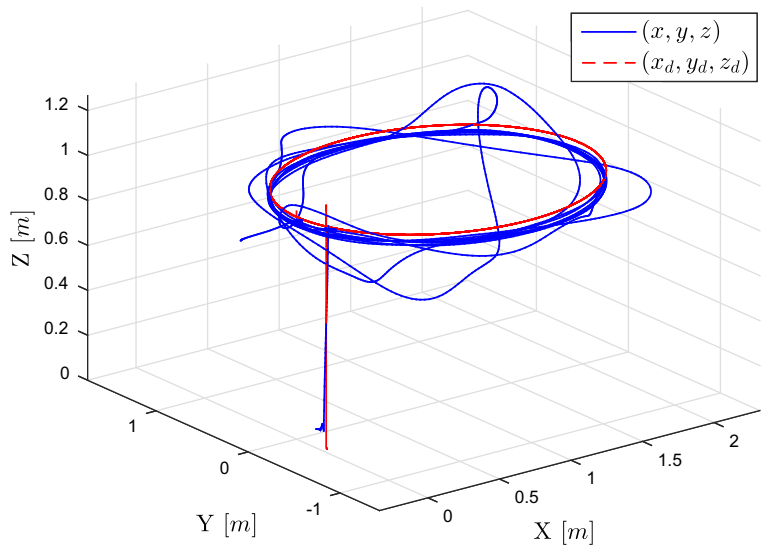

Fig. 38 Quad-rotor's disturbed trajectory in case 2 experiments

Finally, introducing Eq. 30 into Eq. 27 and applying dynamic programming, it follows that

$$0 = \frac{\partial}{\partial(U-G)}\Big[+K_E\bar{H}\dot{\bar{\xi}}^T G + \dot{\bar{\xi}}^T K_p\bar{\xi} + \dot{\bar{\xi}}^T K_T\dot{\bar{\xi}} + x^T Qx\left(K_E\bar{H}\dot{\bar{\xi}}^T M + \dot{\bar{\xi}}^T K_m + \bar{\xi}^T K_T\right)M^{-1} \times (U-G) + (U-G)^T R(U-G)\Big] \quad (31)$$

Then,

$$K_E\bar{H}\dot{\bar{\xi}}^T + (\dot{\bar{\xi}}^T K_m + \bar{\xi}^T K_T)M^{-1} + R(U-G) = 0 \quad (32)$$

Therefore, the control law can be represented as

$$U = -R^{-1}[K_E\bar{H}\dot{\bar{\xi}} + (\dot{\bar{\xi}}^T K_m + \bar{\xi}^T K_T)M^{-1}] + G \quad (33)$$

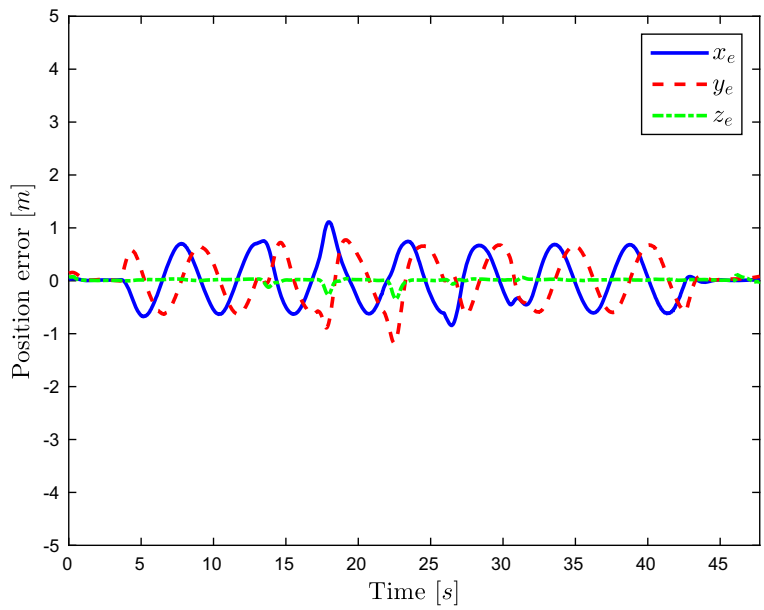

Fig. 39 Quad-rotor's position error in case 1 perturbed flights

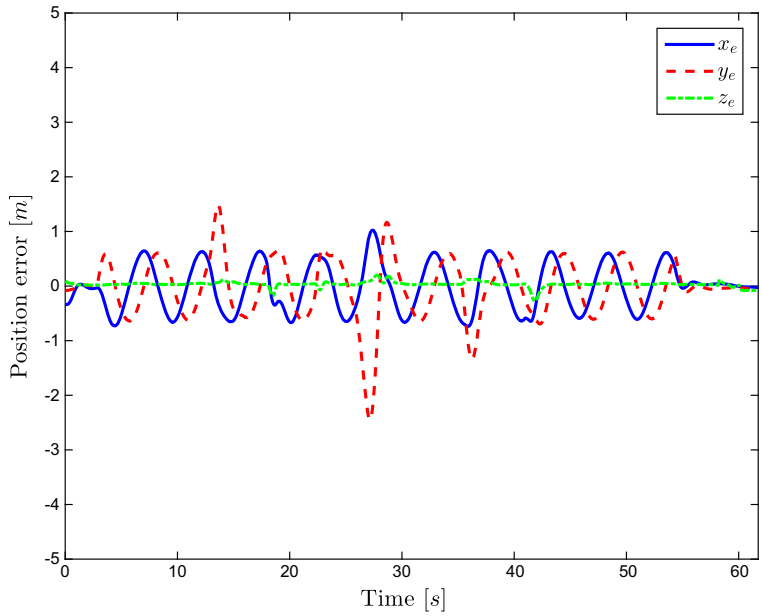

Fig. 40 Quad-rotor's position error in case 2 perturbed flights

The final control law can be rewritten, as follows

$$\begin{bmatrix} F_u \\ \tau_u \end{bmatrix} = R^{-1} \left[M^{-1} \begin{bmatrix} -K_{pt}(p - p_d) - K_{vt}(\dot{p} - \dot{p}_d) \\ -2K_{pr} \ln(\boldsymbol{q}_e) - K_{vr}(\dot{\bar{\theta}} - \dot{\bar{\theta}}_d) \end{bmatrix} - K_E \bar{H} \begin{bmatrix} (\dot{p} - \dot{p}_d) \\ (\dot{\bar{\theta}} - \dot{\bar{\theta}}_d) \end{bmatrix} \right] + \begin{bmatrix} -m\bar{g} \\ 0 \end{bmatrix}$$

Remember that $\bar{\theta}_d = 2 \ln \boldsymbol{q}_d$ and $q_e = \boldsymbol{q} \otimes \boldsymbol{q}_d^*$.

5 Numerical Validation

Our laboratory has developed a simulator which is fully compatible with our drones, and models in a very precise way the dynamics of the UAV, see Fig. 3. Numerical simulations were used to validate both of the proposed control schemes using this simulation environment.

Our platform uses an optical tracking system to measure the vehicle's position with an array of cameras. The references are considered to be in the NED (North-East-Down) convention, where the x axis is pointing the front of the drone, the y points its right side, and the z axis points down.

The control gains were considered to be diagonal matrices, and were adjusted empirically to obtain a stable behavior of the simulation.

$$\begin{array}{ll} K_{pt} = \text{diag}(0.25, 0.25, 2) & K_{pr} = \text{diag}(6, 6, 6) \\ K_{vt} = \text{diag}(0.125, 0.125, 0.5) & K_{vr} = \text{diag}(0.5, 0.5, 1) \\ K_m = \text{diag}(mI^{3\times 3}, J) & K_E = 0.05 \end{array}$$

The UAV platform was considered geometrically symmetric such that the mass and the inertial matrix can be defined as

$$J = \begin{bmatrix} 0.177 & 0 & 0 \\ 0 & 0.177 & 0 \\ 0 & 0 & 0.354 \end{bmatrix}, \quad m = 408\, g$$

5.1 Simulated Scenario

A trajectory was computed such that the vehicle follows a circular path in the horizontal plane while maintaining a constant altitude. The reference points were calculated as

$$p_d = \begin{bmatrix} -r\cos(t_c) + r \\ -r\sin(t_c) \\ z_d \end{bmatrix}, \tag{34}$$

where t_c represents a discrete time which starts in zero when the trajectory begins and increments in

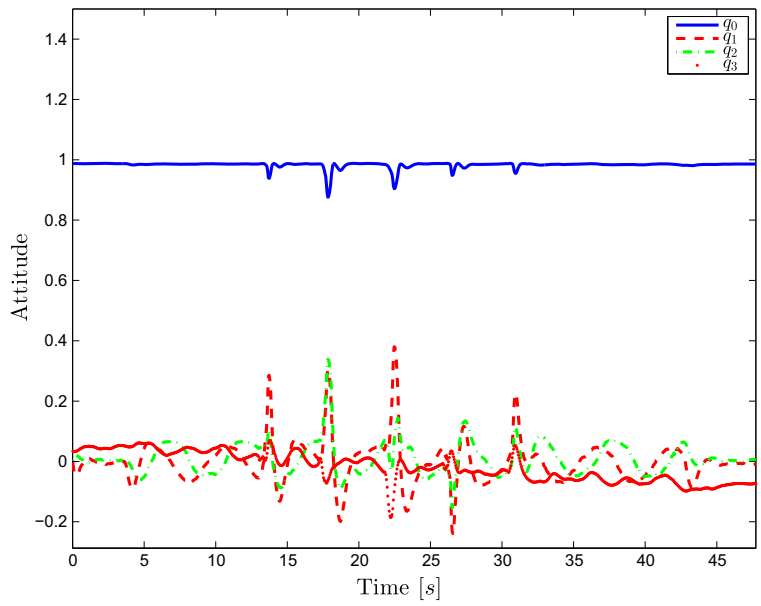

(a) Quad-rotor attitude (q).

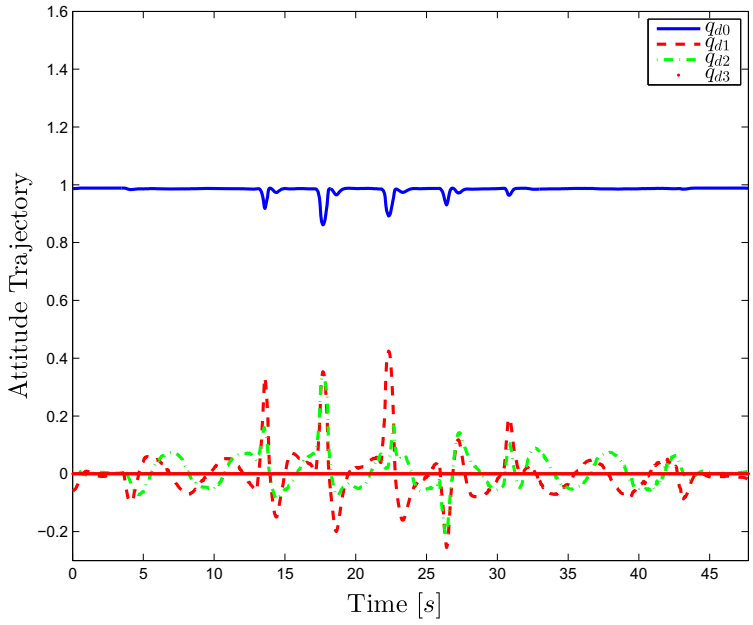

(b) Quad-rotor attitude trajectory (q_d).

Fig. 41 Vehicle's attitude and reference quaternions for case 1 perturbed flights

steps of $\Delta t_c = 0.006$ in each computer cycle, and z_d is the desired altitude which is considered to be constant.

For this simulation, a $r = 1m$ circle was considered for the first two loops, then the radius was abruptly changed to $r = 2m$ until two more loops are made, as illustrated in Figs. 4 and 5.

The position signals and references were used to compute a desired force, depicted in Figs. 6 and 7, to drive the vehicle towards the trajectory.

Fig. 42 Vehicle's attitude and reference quaternions for case 2 perturbed flights

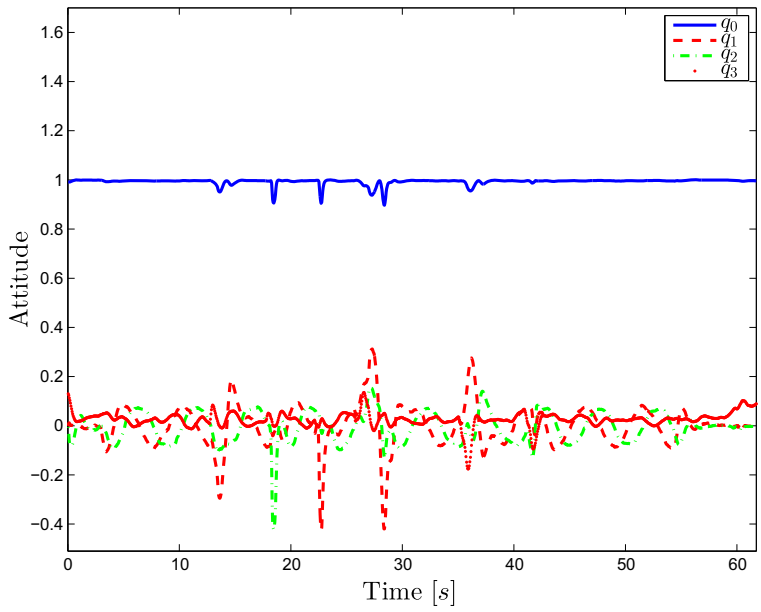

(a) Quad-rotor attitude (q).

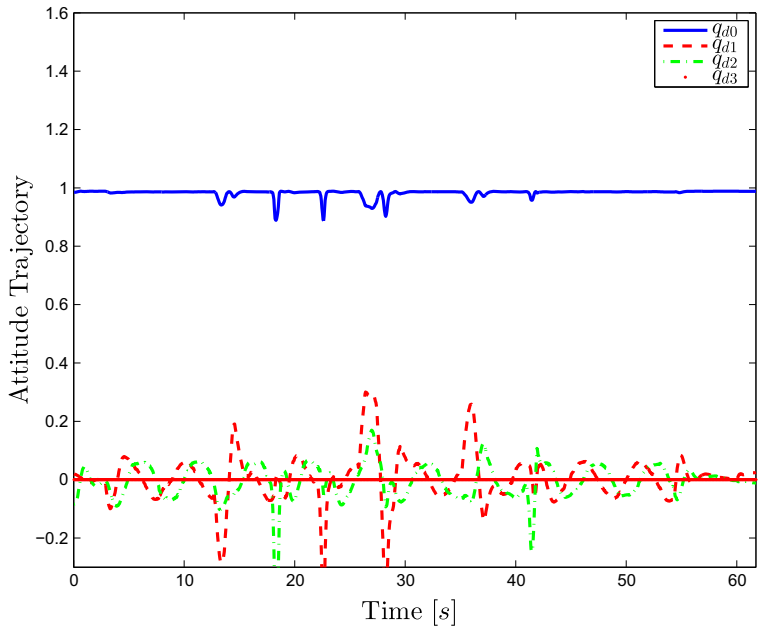

(b) Quad-rotor attitude trajectory (q_d).

The values of these graphs express the fraction of the total force the quadrotor's propellers are able to exert, with $||F_x||, ||F_y||, ||F_z|| < 1$, where 1 means the motors are rotating at their maximum speed.

Using Eq. 24, an attitude trajectory is computed to make the thrust force coincide with the desired force, these trajectories are illustrated in Figs. 8 and 9 alongside with the vehicle's attitude, note the similarity between the orientation quaternion and the trajectory references.

In order to illustrate the attitude behavior in a more comprehensive manner for the reader, a conversion from quaternion to Euler angles was applied as

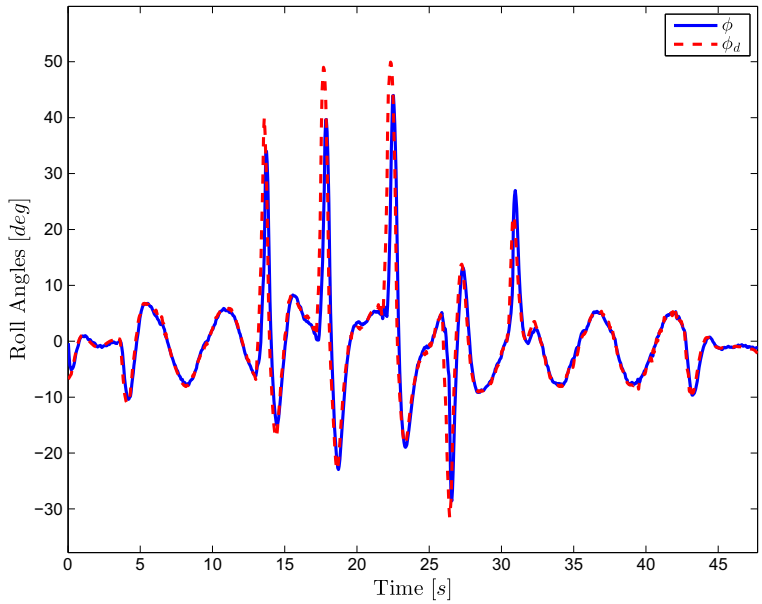

Fig. 43 ϕ angles in case 1 experiments

$$\begin{aligned} \phi &= \text{atan2}\big(2(q_0q_1 + q_2q_3), 1 - 2(q_1q_1 + q_2q_2)\big) \\ \theta &= \text{asin}\big(2(q_0q_2 - q_1q_3)\big) \\ \psi &= \text{atan2}\big(2(q_0q_3 + q_1q_2), 1 - 2(q_2q_2 + q_3q_3)\big) \end{aligned}, \quad (35)$$

The roll, pitch, and yaw angles are illustrated in Figs. 10, 11, 12, 13, 14, and 15.

The rotational inputs are calculated such that $\boldsymbol{q}$ follows $\boldsymbol{q}_d$. Similarly to the input forces, torques are expressed in values $||\tau_x||, |\tau_y||, ||\tau_z|| < 1$, where 0 means no torque and ± 1 means the maximum moment in either direction (Figs. 16 and 17). Finally, the combined torques and forces stabilize the translational error (the difference between the vehicle's position and its reference), represented in Figs. 18 and 19. Note the error values are bounded while describing the circular trajectory, and converge to zero at the

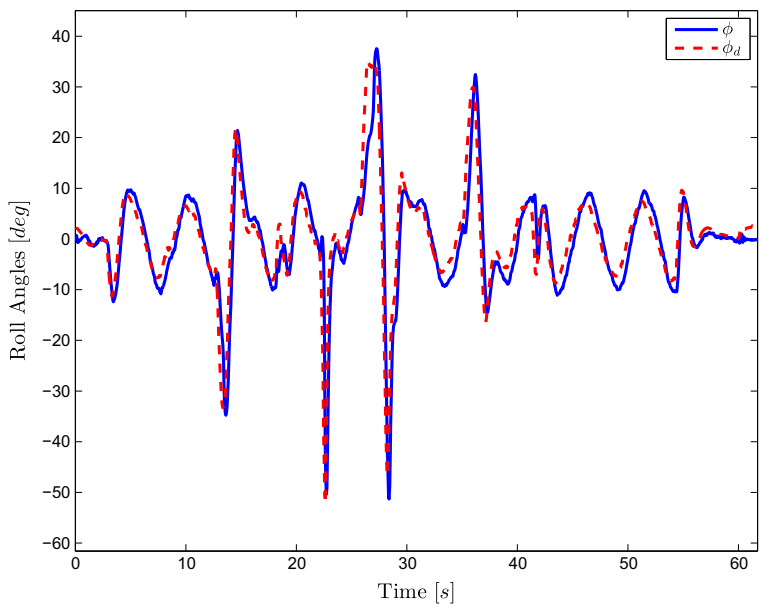

Fig. 44 ϕ angles in case 2 experiments

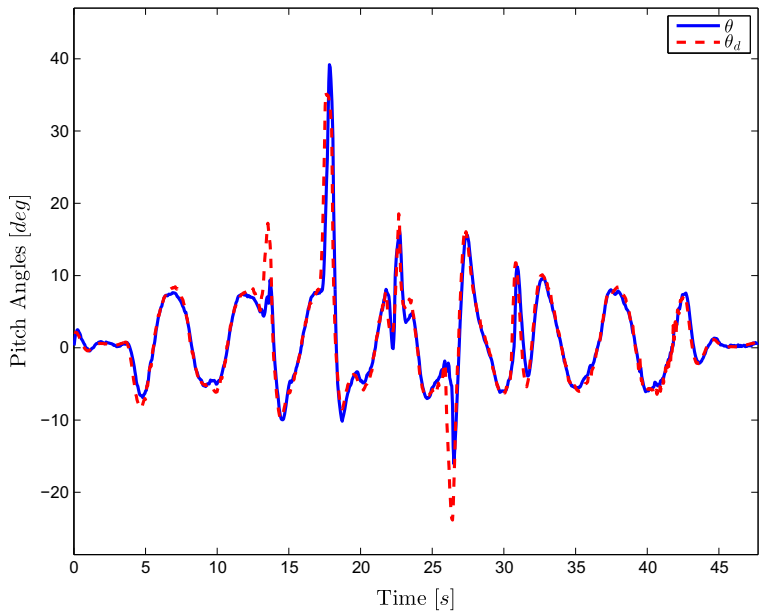

Fig. 45 θ angles in case 1 experiments

end, when the position reference is constant. This validates the presented control laws for both proposed cases.

6 Flight Tests

The Parrot AR Drone 2 was then used to perform tests in real experiments, this UAV has been adapted to work under our laboratory's framework. An Inertial Measurement Unit (IMU), and an OptiTrack motion capture system were used to measure the rotational and translational position and velocities.

6.1 Circular Trajectory

A $r = 1m$ circular trajectory immediately followed by another one with $r = 1.5m$, was introduced to

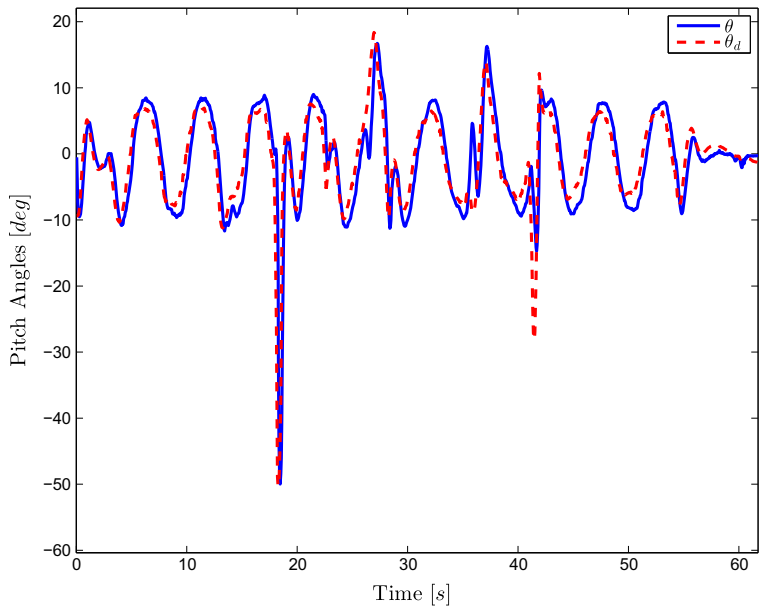

Fig. 46 θ angles in case 2 experiments

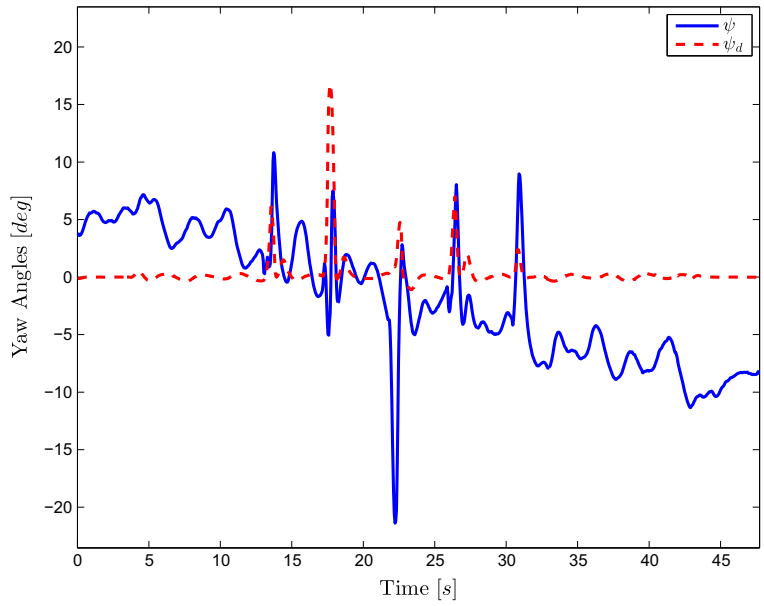

Fig. 47 ψ angles in case 1 experiments

the quadrotor. This is illustrated in Figs. 20 and 21, rotated to the North-West-Up convention for a better appreciation.

The control force is computed using the position error, this is represented in Figs. 22 and 23.

A quaternion attitude trajectory is computed to orient the thrust force to the direction of the control force using the designed controller, which is followed by the vehicle's orientation, this comparison is illustrated in Figs. 24 and 25.

The equivalent Euler Angles were obtained using Eq. 35, and depicted in Figs. 26, 27, 28, 29, 30, and 31.

The torques used to control the quadrotor's attitude are illustrated in Figs. 32 and 33, while Figs. 34 and 35 represent the position error stabilization.

6.2 Perturbed Flights

To further validate our proposal, additional flight tests were added with significant perturbations. The UAV

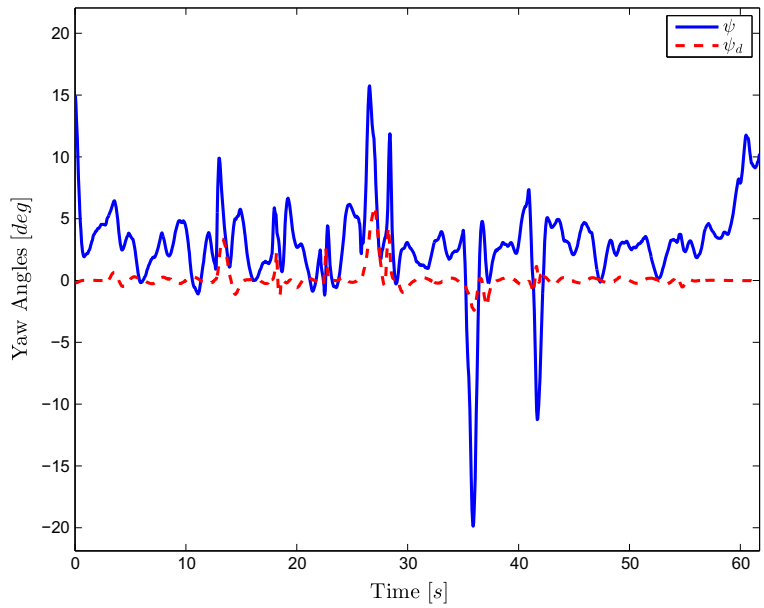

Fig. 48 ψ angles in case 2 experiments

was set to follow a $r = 1m$ circular path, then a member of our team pushed the quadrotor by hand, this push deviates the vehicle from its trajectory (Fig. 36).

The control laws manage to compensate the disturbance and return the drone to its path.

Figures 37 and 38 illustrate the desired trajectory and the disturbed path taken by the quadrotor. The errors are presented in Figs. 39 and 40.

The quaternion orientation trajectory and the UAV's attitude are compared in Figs. 41 and 42. Note the desired attitude reference adjusts when a disturbance is presented. Following Eq. 35, the Euler angles were computed and illustrated in Figs. 43, 44, 45, 46, 47, and 48.

This experiments helped us test the robustness of our proposed control laws, and we were able to confirm their validity even when important disturbances are present.

The described tests were recorded in a video that can be watched in the following link: https://youtu.be/z35Ti_wLRro.

7 Conclusions

In this article, the design of a dynamical model based on Euler-Lagrange formalism using a logarithmic mapping in the quaternion space was introduced. The vehicle attitude is denoted by the axis-angle representation of an unit quaternion. The obtained mathematical model through force $\bar{F}_{th}$ rotated facilitated the control strategy design.

The presented control methods were used to design attitude and also position controllers. These are based on a energy function which has been defined as a Lyapunov function. The proposed controllers present a similar behavior in simulations. However, the control law for case 1 was found to have better performance than the control law of the case 2. The controllers use the quaternion representation of the attitude. Also, the attitude controllers use the quaternion error to compute desired torques.

The proposed control strategies allow the stabilization of the full quadrotor dynamics. The presented methodology eliminates undesired effects such as the gimball-lock or discontinuities, which are common problems using traditional approaches.

Simulations have shown that the performance of the designed algorithms is satisfactory. The presented experiments validate the application of the proposed control laws in a real quadrotor platform with good performance when tracking a desired trajectory and also in presence of disturbances.

Future works include the design of control laws for a quadrotor transporting a cable-suspended payload.

Acknowledgment The authors would like to thank the Mexican National Council for Science and Technology (CONACYT) for their support with the doctoral scholarships program, as well as the French National Network of Robotics Platforms (ROBOTEX).

References

1. Fritsch, O., De Monte, P., Buhl, M., Lohmann, B.: Quasi-static feedback linearization for the translational dynamics of a quadrotor helicopter. In: American Control Conference (ACC), pp. 125–130 (2012)
2. Djamel, K., Abdellah, M., Benallegue, A.: Attitude Optimal Backstepping Controller Based Quaternion for a UAV. Hindawi Publishing Corporation Mathematical Problems in Engineering (2016). Article ID 8573235
3. Chovancová, A., Fico, T., Hubinský, P., Duchon, F.: Comparison of various quaternion-based control methods applied to quadrotor with disturbance observer and position estimator. IEEE Robotics and Autonomous Systems **79**, 87–98 (2016)
4. Tayebi, A., McGilvray, S.: Attitude stabilization of a VTOL quadrotor aircraft. IEEE Trans. Control Syst. Technol. **14**(3), 562–571 (2006)
5. Sanchez, A., Parra-Vega, V., Garcia, O., Ruiz-Sanchez, F., Ramos-Velasco, L.E.: Time-parametrization control of quadrotors with a robust quaternion-based sliding mode controller for aggressive maneuvering. In: European Control Conference (ECC), Zurich, Switzerland, pp. 3876–3881 (2013)
6. Fresk, E., Nikolakopoulos, G.: Full quaternion based attitude control for a quadrotor. In: IEEE European Control Conference (ECC), Zurich, Switzerland (2013)
7. Cariño, J., Abaunza, H., Castillo, P.: Quadrotor Quaternion Control. In: International Conference on Unmanned Aircraft Systems (ICUAS), Denver, USA (2015)
8. Dargham, R., Medromi, H.: Euler and quaternion parameterization in VTOL UAV dynamics with test model efficiency. International Journal of Applied Information Systems (IJAIS) **9**(8) (2015)
9. Honglei, A., Jie, L., Jian, W., Jianwen, W., Hongxu, M.: Backstepping-based inverse optimal attitude control of quadrotor. Int. J. Adv. Robot. Syst. **10** (2013). doi:10.5772/56337
10. El-Badawy, A.A., Bakr, M.A.: Quadrotor aggressive maneuvers along singular configurations: an energy-quaternion based approach. Journal of Control Science and Engineering, 7324540 (2016)

11. Fritsch, O., Tromba, D., Lohmann, B.: Cascaded energy based trajectory tracking control of a quadrotor. Automatisierungstechnik **62**(6), 408–422 (2014)
12. Guerrero, M.E., Lozano, R., García, C.D.: Control Basado En Pasividad Para Un Quadrotor UAV. In: IEEE Congreso Nacional De Control Automático (AMCA), Morelos, Mexico (2015)
13. Souza, C., Raffo, G.V., Castelan, E.B.: Passivity based control of a quadrotor. In: 19th World Congress the International Federation of Automatic Control (IFAC) Cape Town, South Africa, pp. 24–29 (2014)
14. Muñoz, L.E., Santos, O., Castillo, P., Fantoni, I.: Energy-based nonlinear control for a quadrotor rotorcraft. In: American Control Conference (ACC), Washington, DC, USA, pp. 1177–1182 (2013)
15. Kottenstette, N., Porter, J.: Digital passive attitude and altitude control schemes for quadrotor aircraft. In: IEEE International Conference on Control and Automation (ICCA), Christchurch, New Zealand, pp. 1761–1768 (2009)
16. Spring, K.W.: Euler parameters and the use of quaternion algebra in the manipulation of finite rotations: a review. Mech. Mach. Theory **21**(5), 365–373 (1986)
17. Altmann, S.L.: Hamilton, Rodrigues, and the quaternion scandal. Math. Mag., 291–308 (1989)
18. Campa, R., Camarillo, K.: Unit quaternions: a mathematical tool for modeling, path planning and control of robot manipulators. In: Ceccarelli, M. (ed.) Robot Manipulators, In-Teh, pp. 21–48 (2008)
19. Kuipers, J.B.: Quaternions and Rotation Sequences, vol. 66. Princeton University Press, Princeton (1999)

Maria-Eusebia Guerrero-Sánchez was born in Veracruz, Mexico, on April 11, 1984. He received the M.Sc. degree in electronic engineering from the Centro Nacional de Investigación y Desarrollo Tecnológico (CENIDET), Morelos, Mexico, in 2008 and the Ph.D. degree in automatic control from the Department of Electronics Engineering at Centro Nacional de Investigación y Desarrollo Tecnológico. His research interests are focused on passivity-based control, nonlinear control, underactuated mechanical systems, and autonomous helicopters.

Hernan Abaunza was born in Morelos, Mexico, on October 1, 1990. He received the B. S. degree in mechatronic engineering from the Instituto Tecnologico y de Estudios Superiores de Monterrey (ITESM), Mexico, in 2012, the M. Sc. degree in autonomous systems for aerial and submarine navigation from the Centro de Investigación y de Estudios Avanzados (CINVESTAV), Mexico, in 2014, he is currently working to obtain his Ph.D. degree in Automatic Control from the University of Technology of Compiégne, France. His research topics include real-time control applications, quaternion-based modeling and control, and cooperative navigation between unmanned aerial and ground vehicles.

Pedro Castillo (S'04) was born in Morelos, Mexico, on January 8, 1975. He received the B. S. degree in electromechanic engineering from the Instituto Tecnologico de Zacatepec, Morelos, Mexico, in 1997, the M. Sc. degree in electrical engineering from the Centro de Investigación y de Estudios Avanzados (CINVESTAV), Mexico, in 2000, and the Ph.D. degree in automatic control from the University of Technology of Compiégne, France, in 2004. His research topics include real-time control applications, nonlinear dynamics and control, aerospace vehicles, vision, and underactuated mechanical systems.

Rogelio Lozano was born in Monterrey Mexico, on July 12, 1954. He received the B.S. degree in Electronic Engineering from the National Polytechnic Institute (IPN) of Mexico in 1975, the M.S. degree in Electrical Engineering from CINVESTAV-IPN, Mexico in 1977, and the Ph.D. degree in Automatic Control from LAG, INPG, France, in 1981. His research topics include control and observers for non linear dynamical systems, adaptive control, passive systems, modelling and control of small UAV and localization of UAV using vision systems or radio signals.

Carlos-Daniel García-Beltán was born in San Luis Potosi, Mexico, in 1971. He received the M.Sc. degree in electronic engineering from the Centro Nacional de Investigación y Desarrollo Tecnológico (CENIDET), Morelos, Mexico, in 1991, and the Ph.D. degree in process engineering from the Polytechnical Insitute of Grenoble, France, in 2004. Since 1994, he has held teaching and research positions at the CENIDET, where he mainly works on Intelligent Control, Fault diagnosis, Fault Tolerant Control, Robotics.